MODELS TO ASSESS THE QUALITY OF STORED ERYTHROCYTE SUSPENSIONS BY DIFFUSE REFLECTANCE MEASUREMENTS

by

Osman Melih Can

B.S., in Department of Biomedical Engineering, Yeditepe University, 2010

M.S., in Institute of Biomedical Engineering, Boğaziçi University, 2014

Submitted to the Institute of Biomedical Engineering

in partial fulfillment of the requirements

for the degree of

Doctor

of

Philosophy

Boğaziçi University

2020

ACKNOWLEDGMENTS

First and foremost, I would like to express my sincere gratitude and profound respect to my supervisors, Prof. Dr. Yekta Ülgen and Assoc. Prof. Dr. Bora Garipcan. Despite his retirement from the Institute of Biomedical Engineering in the middle of my PhD study, Prof. Dr. Yekta Ülgen has always guided and supported me with his immense experience and Assoc. Prof. Dr. Bora Garipcan was always with me anytime I need.

I gratefully acknowledge committee members: Prof. Dr. Can Yücesoy and Prof. Dr. Murat Gülsoy for their valuable contributions during periodical thesis progress presentations, Prof. Dr. Ata Akın who was also the one firstly encouraged me to study on this project and Dr. Burcu Tunç Çamlıbel, for sharing their valuable time and insightful comments during dissertation defense.

I would like to thank Turkish Red Crescent, General Directorate of Blood Services for allowing the experiments to held in Northern Marmara Regional Blood Center. I especially thank members of Quality Control Laboratory, in Northern Marmara Regional Blood Center for their assistance during the experiments.

I would like to thank Düzce University for their support during my study in Boğaziçi University.

I would like to thank my colleagues and friends in Institute of Biomedical Engineering: Bengü Aktaş, Fatma Gülden Şimşek Temiz, Gökçe Hale Hatay, Özgen Öztürk Öncel, Öznur Demir Oğuz, Sezin Eren Demirbüken.

The dissertation would not have been possible without the constant support of my wife Sevil Can. I am grateful to her for her endless patience and rising my motivation throughout my research. I would like to thank all my family members;

Cemile, Ahmet and Mithat Can, I am very grateful for having you all.

The study was granted by TÜBİTAK under the code 115E477 and additional financial supports have been provided throughout the study by the program "ÖYP" which is governed by Council of Higher Education (YÖK).

ACADEMIC ETHICS AND INTEGRITY STATEMENT

I, Osman Melih Can, hereby certify that I am aware of the Academic Ethics and Integrity Policy issued by the Council of Higher Education (YÖK) and I fully acknowledge all the consequences due to its violation by plagiarism or any other way.

Name :

Signature:

Date:

ABSTRACT

MODELS TO ASSESS THE QUALITY OF STORED ERYTHROCYTE SUSPENSIONS BY DIFFUSE REFLECTANCE MEASUREMENTS

Legislation in transfusion medicine define hemolysis level as the quality measure for erythrocyte suspensions (ES). Since the golden standard test for hemolysis is destructive and causing wastage of units, the hemolysis levels of ES are currently assessed with deceptive visual inspection method and the national blood banks periodically perform statistical quality analysis by measuring the hemolysis levels of only few units on their expiration dates. There are numerous studies revealing negative consequences of storage lesions on recipients. Therefore, a non-invasive diagnostic technique should be developed for the quality of each stored ES, before administering them to especially critically ill patients. Transparent thin plastic blood bags allow optical measurements. Diffuse reflectance spectroscopy (DRS) can be utilized for rapid and non-invasive evaluation of stored blood quality. The purpose of this study is to create models for predicting the hemolysis level or free hemoglobin (FHB) concentration of ES, with spectral parameters acquired from non-invasive diffuse reflectance measurements. After attempts with mixed model, a physically based exponential theory was used and a model was created with fresh ES having negligible FHB to observe the effect of hematological variables on the diffuse reflectance spectra. High levels of goodness of fits were observed ($R^2 \simeq 0.93$). A semi-empirical equation, expressing the reflectance as a linear function of the reduced scattering coefficient of ES, was utilized. Its validity was confirmed with Monte Carlo simulations. Finally, FHB concentrations in ES were modeled as the linear function of the reflectance and other hematological variables. The highest correlation coefficient between predicted and actual FHB concentrations was 0.89. The error rate of the model in diagnosis was about 10%.

Keywords: Diffuse Reflectance, Scattering, Modeling, Hemolysis, Free Hemoglobin, Erythrocyte Suspension, Transfusion.

ÖZET

SAKLANAN ERİTROSİT SÜSPANSİYONLARININ KALİTESİNİ DAĞINIK YANSIMA ÖLÇÜMLERİ İLE TEŞHİS EDEN MODELLER

Transfüzyon tıbbındaki mevzuat, hemoliz seviyesini eritrosit süspansiyonları (ES) için kalite ölçüsü olarak tanımlar. Hemoliz ölçümünde altın standart test, yıkıcı ve ünitelerin israfına neden olduğundan, ES'nin hemoliz seviyesi şu anda yanıltıcı görsel muayene yöntemi ile değerlendirilmektedir ve ulusal kan bankaları periyodik olarak sadece birkaç ünitenin hemoliz seviyelerini son kullanma tarihlerinde ölçerek istatistiksel kalite analizi yapmaktadır. Depolama lezyonlarının alıcılar üzerindeki olumsuz sonuçlarını ortaya koyan çok sayıda çalışma vardır. Bu nedenle, saklanan her ES'nin özellikle kritik hastalara aktarılmadan önce kalitesini değerlendirmek için girişimsel olmayan bir tanı tekniği geliştirilmelidir. Şeffaf ve ince plastik torbalar, optik ölçümlere izin verir. Depolanan kan kalitesinin hızlı ve girişimsel olmayan bir şekilde izlenmesi için dağınık yansıma (DY) ölçümleri kullanılabilir. Bu çalışmanın amacı, girişimsel olmayan DY ölçümlerinden elde edilen spektral parametrelerle ES'nin hemoliz seviyesini veya serbest hemoglobin (FHB) konsantrasyonunu tahmin etmek için modeller oluşturmaktır. Karma model denemelerinden sonra, fiziksel temelli bir üstel teori kullanılmış ve hematolojik değişkenlerin DY spektrumları üzerindeki etkisini gözlemlemek için ihmal edilebilir FHB'ye sahip taze ES'ler ile bir model oluşturulmuştur. Yüksek düzeyde uyum iyiliği gözlenmiştir ($R^2 \simeq 0.93$). ES'nin indirgenmiş saçılma katsayısının doğrusal bir fonksiyonu olarak yansıtma sağlayan yarıdeneysel bir model kullanılmıştır. Bu modelin geçerliliği Monte Carlo simülasyonları ile teyit edildi. Son olarak, ES'deki FHB konsantrasyonu DY ölçümleri ve diğer hematolojik değişkenlerin doğrusal fonksiyonu olarak modellenmiştir. Tahmin edilen ve gerçek FHB konsantrasyonları arasındaki en yüksek korelasyon katsayısı 0.89'dur. Teşhiste modelin hata oranı yaklaşık % 10'dur.

Anahtar Sözcükler: Dağınık Yansıma, Saçılma, Modelleme, Hemoliz, Serbest Hemoglobin, Eritrosit Süuspansiyonu, Transfüzyon.

TABLE OF CONTENTS

LIST OF FIGURES

LIST OF TABLES

LIST OF SYMBOLS

L*	Coordinate of color space corresponds brightness
a*	Coordinate of color space corresponds redness and greenness
b*	Coordinate of color space corresponds blueness and yellowness
A_{415}	Absorbance at 415 nm
A_{380}	Absorbance at 380 nm
A_{450}	Absorbanve at 450 nm
Y_{ij}	Dependent variable of jth sample in the ith measurement
X_{ij}	Independent variable of jth sample in the ith measurement
e_{ij}	Residual error of the jth sample in the ith measurement
i	Index corresponds to repeated measurements
j	Index corresponds to sample
$\mathbf{U_{uncon}}$	Random factors (without 2^{nd} level predictor)
$\mathbf{U_{0,uncon}}$	Standard deviations of intercepts (without 2^{nd} level predictor)
$\mathbf{U_{1,uncon}}$	Standard deviations of slopes (without 2^{nd} level predictor)
$\mathbf{U_0}$	Standard deviations of intercepts (with 2^{nd} level predictor)
$\mathbf{U_1}$	Standard deviations of slopes (with 2^{nd} level predictor)
$\mathbf{Z_0}$	Sample specific predictor for estimating intercepts
$\mathbf{Z_1}$	Sample specific predictor for estimating slopes
$\mathbf{U}$	Random factors
R	Reflectance
dR	Derivative of reflectance
g	Anisotropy factor
L	Radiance
$\mathbf{r}$	Represents an arbitrary location
P	Probability density function
I_0	Intensity of the incident light
I_R	Intensity of the reflected light
z	Coordinate axis

L_{bag}	Thickness of the bag
dz	Infinitesimally small layer
R_d	Diffuse reflectance
R_m	Measured diffuse reflectance
k_1	First calibration factor
k_2	Second calibration factor
k_3	Third calibration factor
k_4	Fourth calibration factor
H	Hematological variable
n	Index corresponding particle types in ES
c_n	Concentration of particle n in ES
V_n	Volume of particle n in ES
R_{norm}	Normalized diffuse reflectance
$\mathbf{X}$	Design matrix
$\mathbf{b}$	Vector of regression coefficients
$\mathbf{e}$	Vector of residual errors
$\mathbf{Y}$	Vector of outcome variable
$\mathbf{X_p}$	Predictor of the design matrix
p	Index corresponds to the number of predictors
c	Concentration
DL	Detection Limit
s	Slope of the calibration line
QL	Quantification Limit
β_{0j}	Sample specific intercept for sample j
β_{1j}	Sample specific slope for sample j
$\boldsymbol{\beta_0}$	Vector of sample specific intercepts
$\boldsymbol{\beta_1}$	Vector of sample specific slopes
$\gamma_{00,uncon}$	Mean of intercepts in model lack of 2^{nd} level predictor
$\gamma_{10,uncon}$	Mean of slopes in model lack of 2^{nd} level predictor
γ_{00}	First regression coefficient corresponding to the intercept

γ_{01}	Second regression coefficient
γ_{10}	Third regression coefficient
γ_{11}	Fourth regression coefficient
$\sigma_{explained}$	Standard deviation explained by the 2nd level predictor
λ	Wavelengths
μ_a	Absorption coefficient
μ_s	Scattering coefficient
$\hat{\boldsymbol{\omega}}$	Represents an arbitrary direction
μ_t	Total attenuation coefficient
$\hat{\boldsymbol{\omega}}'$	Represents a direction, other than $\hat{\boldsymbol{\omega}}$
$\mathrm{d}\hat{\boldsymbol{\omega}}$	Represents a solid angle at direction, $\hat{\boldsymbol{\omega}}$
μ_s'	Reduced scattering coefficient
$\mu_{s,bag}'$	Reduced scattering coefficient of blood bag
$\mu_{a,bag}$	Absorption coefficient of blood bag
$\mu_{s,bag}'$	Reduced scattering coefficient of erythrocyte suspension
$\mu_{a,bag}$	Absorption coefficient of erythrocyte suspension
ϵ_{Hb-O_2}	Extinction coefficient of oxygenated hemoglobin
ϵ_{Hb}	Extinction coefficient of unbound hemoglobin
$\sigma_{s,n}$	Scattering cross-section of the particle n
$\mu_{s,RBC}$	Scattering coefficient contributed by red blood cells
$\mu_{s,PLT}$	Scattering coefficient contributed by platelets
$\mu_{s,WBC}$	Scattering coefficient contributed by white blood cells
$\mu_{s,EXT}$	Scattering contributed by the particles in extracellular space
$\gamma(HCT)$	Hematocrit dependent correction factor
$\sigma_{s,RBC}$	Scattering cross-section of red blood cells
σ_s'	Reduced scattering cross-section
σ_s	Scattering cross-section
$\mu_{s,WBC}$	Reduced scattering coefficient of white blood cells
$\mu_{s,EXT}$	Reduced scattering coefficient of extracellular space
$\mu_{s,RBC}$	Reduced scattering coefficient of red blood cells
$\mu_{s,PLT}$	Reduced Scattering coefficient of platelets

σ	Standard deviation

LIST OF ABBREVIATIONS

ES	Erythrocyte suspension
DRS	Diffuse reflectance spectroscopy
FHB	Free hemoglobin
ATP	Adenosine triphosphate
DPG	Diphosphoglycerate
NLR-ES	Non-leukoreduced erythrocyte suspension/s
LR-ES	Leukoreduced erythrocyte suspension/s
NIR	Near infrared
SAGM	Saline-adenine-guanine-mannitol
THB	Total hemoglobin concentration/s
MCHC	Mean cell hemoglobin concentration
HCT	Hematocrit
#RBC	Number of red blood cells
#PLT	Number of platelets
#WBC	Number of white blood cells
MCV	Mean red blood cell volume
MPV	Mean platelet volume
RDW-CV	Radius distribution width-coefficient of variation
RDW-SD	Radius distribution width-standard deviation
PDW	Platelet distribution width
PCT	Plateletcrit
ANOVA	Analysis of Variance
CIELab	A color space
D	Day
RTE	Radiative transport equation
Hb	Unbounded hemoglobin
Hb-O_2	Oxygenated hemoglobin
$SatO_2$	Hemoglobin oxygen saturation level

RMSE	Root Mean Squared Error/s
IAD	Inverse Adding Doubling
GLM	Generalized Linear Model/s
FP	False Positive
TP	True Positive
TN	True Negative
FN	False Negative
SD	Standard Deviation/s
CV	Coefficient of Variation/s

1. INTRODUCTION

1.1 Background

Since the early efforts of direct infusion of human blood from donor's vein to patient's, which were accompanied by a high rate of mortality, in 1820s [1], transfusion of stored blood has become a routine medical treatment saving hundred millions of lives worldwide annually. Discovery of blood group antigens, development of anticoagulant and preservative solutions for lengthening the shelf life of the donated blood and conversion of reusable glass bottles to plastic bags for sterility were definitely the milestones of the 20^{th} century in transfusion medicine [2]. In recent decades, stringent screening of donors, serological and nucleic acid amplification tests have nearly eliminated the transmission risk of infectious diseases and prestorage leukocyte depletion, rejuvenation, red cell washing, gamma irradiation have minimized immune-mediated reactions in recipients [3]. Not withstanding of these ameliorations, there is still room for further optimizing the quality, safety and efficacy of blood transfusion.

Red blood cells do not evolve to cope with chemical and mechanical stresses under hypothermic conditions isolated from the circulation and encounter serious physiological and morphological changes over time during ex vivo storage, called "storage lesions" [4]. Storage lesions include the decrease of adenosine-triphosphate (ATP), pH and 2,3-diphosphoglycerate (DPG) levels, of which the latter has a role in stabilizing hemoglobin oxygen affinity, and the subsequent oxidative damages to red cells causing shape changes, membrane losses and the decline in rheological properties such as deformability, and the eventual disruption of red cells following accumulation of microvesicles, heme, iron and free hemoglobin (FHB) into the extracellular medium [5]. Although the clinical impact of storage lesions remain as a matter of debate, these impairments, in general, reduce the viability of stored red cells and have been impugned as the cause of adverse outcomes [6] reported in a numerous retrospective studies [7, 8, 9, 10, 11, 12, 13, 14, 15, 16]. Even the use of leukoreduced units yielded

similar results [17, 18, 19, 20, 21, 22], whereas a few observational studies [23, 24, 25], systematic reviews [26, 27, 28] and multi-center randomized clinical trials [29, 30, 31] showed no beneficial effect of fresh blood versus stored blood.

The primary indication of transfusion is not only restoring the capacity of oxygen carriers in patient's circulation, but more importantly improving the oxygen delivery to tissues. However, impaired rheological properties of stored red cells [32]; increased rigidity, aggregability, osmotic fragility [33] and adhesion to vascular endothelium may affect the blood flow [34]. Normal red cells are flexible to adapt their shape for passing through the capillaries that have two to three-fold narrower than their diameters. Rigid, poorly deformable and aggregated red cells may be entrapped in the microcirculation of the patient [35]. The elevated adhesion of red cells to endothelial cells of the vessel wall may lead to flow disturbances by increasing resistance in large vessels or direct blockage in the capillaries [36]. Although the majority of the mechanically damaged cells can be cleared from the bloodstream via the recipient's reticuloendothelial system, a small fraction of these cells lose their integrity and release FHB which inhibit vasodilatory activity and impact blood flow [4]. Substantially, in vitro storage-induced hemolysis escalate FHB concentrations in transfused patient. Together with membrane encapsulated hemoglobin, in the form of microvesicles, FHB molecules scavenge nitric oxide, which is a signaling molecule modulating vasodilation [37]. Besides, they potentiate neutrophils, macrophages and other mechanisms of innate immune system and injure tissue or organs through inflammation [38, 39]. These deleterious effects of FHB and dysfunctional red cells on microcirculatory flow and oxygen perfusion were supported by animal models [40, 41, 42] and clinical studies [43, 44, 45].

1.2 Motivation and Aim

Legislation in transfusion medicine recognize hemolysis level of stored red cell units as a quality measure and the current quality standard established by the regulatory agencies in Europe requires that at the end of the approved storage period, ES should have hemolysis levels less than 0.8% [46], while audits in America recommends

1.0% for the accepted limit of hemolysis level [47]. The national blood banks must show that 95% of blood products meet the standard with 95% confidence level [48]. For the statistical quality check, limited number of blood products are randomly selected from the pool and their hemolysis levels are controlled on their expiry date [46]. Since the test method is destructive and leading wastage of controlled products, it is not applicable to all units. Currently, the only method for quality evaluation of units, prior to transfusion, involves physical examination and visual inspection of hemolysis [49]. The redness of the suspending fluid, when the red cells settle, serves as a marker of hemolysis. The presence of FHB, turns the color of cell-free media from yellow to pink. In case of excessive FHB concentrations, the color becomes dark red [49]. Nevertheless, visual assessment of hemolysis level is subjective and mostly decisive [50].

Today's practice of quality management is inadequate for a plenty of reasons. Firstly, hemolysis levels of units are subject to variations due to genetic factors of the donor [51]. High donor variations in end-of-storage hemolysis have shown in previous studies [52, 53] and therefore statistical estimation of stored blood quality would be insufficient. Secondly, the intention of the current quality control system is to ensure good manufacturing practices in blood collection, processing and standard storage, but units may undergo unusual conditions during storage; gamma irradiation, cell washing, temperature fluctuations due to transportation. The effect of these processes on blood quality is not controlled. Moreover, according to massive transfusion protocols, units are issued to emergency or operation rooms, but many of them return unused [54, 55]. For such situations, a historical 30-minute rule is decisive for discarding or keeping the returned units [56]. Rather than the traditional methods, the quality of each unit can be measured by utilizing of biomedical diagnostic technologies. Without invading the bag and contaminating the blood, transparent plastic bags would allow optical based measurements. Such non-invasive techniques may provide continuous monitoring of units until their administration.

There are a number of studies targeting this idea, Meinke et. al. introduced an optical device that utilizes the transmittance of the light through the tube of the bag [57]. This system needs settlement or centrifugation of the red cells before the

application. Spatially offset Raman spectroscopy has been studied to monitor the biochemical changes in the bag [58, 59]. Feasibility of photoacoustic imaging method was recently introduced by Pinto et. al. [60]. In our previous study, color parameters of 7 non-leukoreduced erythrocyte suspensions (NLR-ES) were observed during 42 days and it was found that some of the parameters were moderately correlated with the hemolysis level in the bag [61].

In this dissertation, diffuse reflectance spectroscopy (DRS) as a rapid, low cost, non-invasive diagnostic tool is proposed to assess the quality of stored blood by estimating the FHB concentration in the blood bag. The aim is to create models for accurately predicting quality related parameters of stored blood with non-invasive diffuse reflectance measurements. Following Chapters include the analysis on diffuse reflectance spectra of ES in visible and near infrared (NIR) regions, during an extended storage period for investigating the accuracy of acquired spectral parameters in the models.

1.3 Overview of the Dissertation

In Chapter 2, with the motivation of our previous study that showed moderate correlation between color parameters and hemolysis level of blood [61], a linear mixed model was constructed to relate FHB concentration and optical measurements. Hematological variations in blood samples were used to explain the random errors of the model.

In Chapter 3, instead of statistical regression models, a physically based exponential theory of diffuse reflectance derived from RTE, was introduced. The reflectance theory was examined on 103 fresh ES units that have negligible FHB concentrations. Diffuse reflectance of units were modeled with absorption and scattering coefficient of blood, which were then replaced with hematological parameters, by non-linear least squares regression. The effect of optical properties of the blood bag were also investigated in Chapter 3.

In Chapter 4, leukoreduced erythrocyte suspensions (LR-ES) were exposed for prolonged storage period and red cells were spontaneously hemolyzed during the storage. The light scattering characteristics of blood were partitioned in a way that each cell contributed to scattering coefficient of blood according to the ratio of their total volume in the suspension to their average size. A semi-empirical diffuse reflectance equation was introduced in order to highlight the scattering contribution of extracellular medium in blood mainly caused by increased FHB concentration. The semi-empirical equation expressed reflectance as a linear function of the optical properties of blood. Finally, the FHB concentrations and the hemolysis levels of blood were modeled with ES in the training set and FHB concentrations of ES in the validation set were estimated accurately, according to the acquired model.

Chapter 5 concludes the dissertation with the general discussion.

Appendices include performance tests of diffuse reflectance measurements. The repeatibility, consistency and sensitivity analysis of the measurements were performed.

2. REPEATED MEASURES APPROACH

2.1 Background and Objectives

Previous studies have shown that the color parameters obtained from diffuse reflectance spectrum of ES measured over blood bag, changed during the storage period. A specific increase was observed in the coordinate axes of color spaces representing redness of the reflected light from the bag. This increase was in correlation with the hemolysis level of the stored unit, measured in the laboratory by sampling blood from the bag. The correlation coefficient was around 0.7. However, there existed variations between blood color parameters recorded on the first day of the storage [61]. The main reason was possibly the variations in the hematology of each unit; e.g. hemoglobin concentration, hematocrit. The precision of the model for quality prediction could be improved by the inclusion of these hematological variables. The objective of this study was to model hemolysis level or FHB concentration of the blood with the parameters obtained from diffuse reflectance measurements and the hematological variables of the units. Disparate from Ref. [61], in this study the units were monitored mainly beyond 42 days of normal storage period, to generate wider range of hemolysis levels due to the extended storage.

2.2 Methodology

2.2.1 Samples

In this study, 24 NLR-ES and 28 LR-ES were employed and supplied by the quality control department of Northern Marmara Regional Blood Center with the permission of Turkish Red Crescent. The units were prepared from whole blood of healthy donors. As in the general preparation process of ES, blood was collected into a multi-bag system prefilled with an anticoagulant containing citrate, phosphate, and dextrose

solution. The collected whole blood was centrifuged and then plasma transferred into a different bag in closed multiple bag system. The remaining blood forms the NLR-ES. LR-ES were produced by directing remaining blood through leukocyte filter. As the final step, a preservative solution, saline-adenine-glucose-mannitol (SAGM), which contains saline, adenine, glucose, mannitol was added for the nourishment of red blood cells during storage [62]. All ES were stored for 70 days.

2.2.2 Experiments

During storage, tests were performed on the 1st, 42nd, 49th, 56th, 63rd and 70th day of the storage. First, the diffuse reflectance and color parameters of ES were measured. Then, 5 ml of blood were drawn from the bags for measuring hematological parameters and hemolysis levels with usual laboratory techniques.

2.2.2.1 Measurement of diffuse reflectance. Prior to measurements, ES were taken out from the refrigerator and kept at room temperature. They were gently shaken for homogenizing cells in the suspension. Blood unit was then placed in a dark black box (Thorlabs, XE25C5D/M) which was used for keeping the ambient light out of the measurement setup. A probe holder (Thorlabs, RPS-SMA) was used to immobilize the blood bag and reflection probe (Thorlabs, RP20). The reflection probe used in this study had a bundle of fiber optic cables and transmitted the light from the source to the bag and collected the reflected light from the bag and transmitted it to the spectrometer. The reflection probe was connected to the probe holder from the 45 degree mount of the probe holder. The source was a tungsten halogen lamp (Ocean Optics, HL-2000) and the spectrometer (Ocean Optics, USB4000) had 3648-element CCD array detector covering wavelengths from 346 nm to 1037 nm. The spectrometer was connected to the computer via USB port and a special software (Ocean Optics, Oceanview) was used to record the reflectance spectrum. The software also calculated the coordinate values: L*, a*, b*, chroma and hue angle of CIELab, color space defined by International Commission on Illumination.

2.2.2.2 Measurement of hematological parameters. After diffuse reflectance measurements, 5 ml of homogeneous blood were drawn from bags. About 10 μl of sampled blood were aspirated by the hematology analyzer (Mindray, BC3000) one by one. The instrument read total hemoglobin concentration (THB) in g/L, mean cell hemoglobin concentration (MCHC) in g/L, hematocrit (HCT), number of red blood cells (#RBC), white blood cells (#WBC) and platelets (#PLT) in one liter of blood, mean red blood cell volume (MCV) and mean platelet volume (MPV) in μm^3, the coefficient of variation of the radius distribution width for red blood cells (RDW-CV), the standard deviation of the radius distribution width for red blood i.cells (RDW-SD) in μm^3, the radius distribution width for platelet cells (PDW)(%) and finally the plateletcrit (PCT)(%).

2.2.2.3 Measurement of hemolysis level. Sampled blood from bags were centrifuged at 3000 rpm, for 20 minutes. Supernatant were taken from tubes and diluted with 0.01 % Na_2O_3 solution to 1:10. The diluted samples were pipetted into a cuvettes. Absorbance relative to distilled water at 380 nm 415 nm, 450 nm were read by a bench-top spectrometer (Beckman Coulter, DU 730). The following expression yielded the FHB concentration [63].

$$FHB(g/L) = 0.836 \times (2A_{415} - A_{450} - A_{380}) \tag{2.1}$$

A_{415} was used, since the hemoglobin absorption is highest at this wavelength. Other wavelengths (A_{380} and A_{450}) were used for correcting turbidity caused by the plasma proteins and lipids, respectively [64].

2.3 Modeling Strategy

The effect of storage on hematological variables and optical parameters were investigated with repeated-measures ANOVA, because the groups of samples, measured at different storage periods were not independent (paired samples). The null-hypothesis

of the repeated measures-ANOVA claims that there were no difference between the mean values of a variable of interest, measured in different weeks. Nonetheless, the repeated measures-ANOVA would reject the null hypothesis even if an output of the variable in one week was significantly different from the outputs in the other weeks. F-statistics was generated as the outcome of the repeated measures-ANOVA, but before the analysis, sphericity of the variables were checked from the double centered covariance matrices of the variables. The null-hypothesis of sphericity test stated that, for a measured variable, the variances between samples were equal in each storage period. Greenhouse-Geisser correction or Huynd-Feldt correction was applied according to the degree of violation on sphericity and probability of the results were calculated from the corrected degrees of freedom values. Type-I error was set as 0.05.

In the modeling, linear mixed regression model was utilized, due to the repeated-measures design. Mixed model is a type of hierarchical model and its main advantage is separating within and between-sample variances in different steps of the hierarchical model [65]. Mixed model would help to test the hypothesis that the relation between the hemolysis level and the optical reflection data would be stronger with addition of between sample variations such as THB, HCT etc. into the model. Therefore, the contribution of sample specific variables were computed by their abilities to reduce random errors of the model.

In the basic form of linear mixed model, the dependent variable Y_{ij} is expressed as a linear function of the independent variable X_{ij}. β_{0j} and β_{1j} are the regression coefficients and e_{ij} is the random error term. The lower indices i and j indicate the number of observations and the number of samples respectively. In other words, Y_{ij} represents the data of sample j at ith measurement. Regression coefficients form the vector of sample specific intercepts and sample specific slopes. The random error term contains the residuals of each sample specific regression lines.

$$Y_{ij} = \beta_{0j} + \beta_{1j} \times X_{ij} + e_{ij} \tag{2.2}$$

β coefficients vary among the samples and at this stage of analysis, the goal is to

explain these variations with sample-wise characteristics. For an unconditional model that does not contain any sample-wise variable, β coefficient vectors of each sample ($\beta_{\mathbf{0}}$ and $\beta_{\mathbf{1}}$) can be separated into their means ($\gamma_{00,\text{uncon}}$, $\gamma_{01,\text{uncon}}$) and the vector of standard deviations ($\mathbf{U}_{0,\text{uncon}}$, $\mathbf{U}_{1,\text{uncon}}$).

$$\boldsymbol{\beta_0} = \gamma_{00,uncon} + \mathbf{U_{0,uncon}} \tag{2.3}$$

$$\boldsymbol{\beta_1} = \gamma_{10,uncon} + \mathbf{U_{1,uncon}} \tag{2.4}$$

These random variances in the unconditional model could be reduced by implementing sample specific variable into the second level:

$$\boldsymbol{\beta_0} = \gamma_{00} + \gamma_{01} \times \mathbf{Z_0} + \mathbf{U_0} \tag{2.5}$$

$$\boldsymbol{\beta_1} = \gamma_{10} + \gamma_{11} \times \mathbf{Z_1} + \mathbf{U_1} \tag{2.6}$$

Here, $\mathbf{U}_0$ and $\mathbf{U}_1$ are the vectors representing between sample variations. $\mathbf{Z}_0$ and $\mathbf{Z}_1$ are the vectors of sample specific variables. γ_{00}, γ_{01}, γ_{10} and γ_{11} are constants and the regression coefficients of the final model. The explained variance ($\sigma^2{}_{\text{explained}}$) with the addition of the sample specific variables can be calculated as:

$$\sigma^2_{explained} = \frac{var(\mathbf{U_{uncon}}) - var(\mathbf{U})}{var(\mathbf{U_{uncon}})} \times 100\% \tag{2.7}$$

2.4 Results

2.4.1 Repeated measures-ANOVA

From the repeated measurements, eight independent hematological variables of 24 NLR-ES and 28 LR-ES were obtained. These hematological variables are THB, HCT, #RBC, #PLT, #WBC RDW-SD, RDW-CV and FHB, the only parameter directly related to blood quality. Others such as MCHC, MCV, hemolysis level can be derived from the independent ones. The outputs of repeated-measures ANOVA

for these hematological variables are given in Table 2.1. FHB concentration was not included in Table 2.1, since the effect of storage on FHB concentration is well-known.

Table 2.1
The outcomes of repeated measures-ANOVA for the hematological variables.

Hematological Parameters	**F-statistics**	**p-value**	**Type of ES**
THB	0.3435	0.79	NLR-ES
	0.8478	0.44	LR
HCT	9.47	<0.001	NLR-ES
	14.6828	<0.001	LR
#RBC	0.6982	0.56	NLR-ES
	1.6385	0.21	LR
#PLT	11.2152	<0.001	NLR-ES
	2.2575	0.078	LR
#WBC	10.2340	<0.005	NLR-ES
	NA	NA	LR
RDW-SD	22.5404	<0.001	NLR-ES
	14.4818	<0.001	LR
RDW-CV	41.0776	<0.001	NLR-ES
	27.1307	<0.001	LR

THB and #RBC did not change during the prolonged storage period, for both NLR-ES and LR-ES. #PLT did not change significantly during the 70 days storage of LR-ES. #WBC could not be tracked in LR samples, but changed significantly in the NLR-ES. The sharpest changes occurred to RDW-SD and RDW-SD. Prolonged storage effect on HCT was also observed. Actually, HCT was a dependent variable and equals the product of #RBC and MCV. Since the #RBC did not change, it was interpreted that MCV was affected by the storage.

Analysis of color space variables are listed in Table 2.2.

The effects of prolonged storage on the measured color parameters varied for NLR-ES and LR-ES. Repeated-measures ANOVA proved that none of the color coordinate values has significantly changed during the storage for NLR-ES, but the weekly

Table 2.2
The outcome of repeated measures-ANOVA for the variables of CIELab.

Color Parameters	F-statistics	p-value	Type of ES
L*	2.2211	0.092	NLR-ES
	2.6426	0.070	LR
a*	0.7951	0.50	NLR-ES
	6.9021	<0.01	LR
b*	0.8980	0.41	NLR-ES
	8.9158	<0.005	LR
chroma	0.7986	0.45	NLR-ES
	7.1627	<0.01	LR
hue-angle	1.1233	0.35	NLR-ES
	11.2641	<0.001	LR

changes in color parameters, except L* were significant for LR-ES.

In the previous study [61], the color coordinate a* of NLR-ES had increased in the period of day 1 to day 42, whereas in this study a* was in decreasing trend after day 42 and did not significantly changed throughout the extended storage period (Table 2.3). In contrast to NLR-ES, the color value a* of LR-ES continued to increase linearly during the entire storage period (Table 2.4). Results show that the color coordinate a* decreased when the hemolysis level was extensively high. Hemolysis levels of NLR-ES exponentially increased after 42nd day, but leukocyte filtration slowed down lysing of red cells and the hemolysis levels of LR-ES beyond their expiration date, could still be as low as the hemolysis level of NLR-ES at the normal storage period (Figure 2.1). Thus, it is supposed that the a* for LR-ES did not decrease during 70 days of storage, because the hemolysis levels of LR-ES were not extensively high in this period.

Another important observation was that the color value a* of LR-ES was higher than the color value a* of NLR-ES-ES. The average and standard deviation (SD) of color value a* for NLR-ES was 10.67 ± 2.83 and it was 16.95 ± 2.85 for LR-ES ($p < 10^{-71}$). Non-invasive color measurements can definitely distinguish NLR-ES and LR-ES.

Table 2.3
Color parameter, a* of 24 NLR-ES measured during prolonged storage, (D=day).

Sample Codes	D1	D42	D49	D56	D63	D70
T********3273	8.36	10.10	10.98	11.09	10.69	10.90
T********3289	12.28	16.23	14.94	14.16	14.09	14.15
T********5388	14.60	17.65	15.78	16.47	16.13	16.88
T********5403	8.49	14.99	12.13	12.95	12.48	13.00
T********5797	6.64	8.19	7.94	8.25	6.10	7.05
T********5803	7.59	9.59	11.36	11.68	12.00	11.89
T********5996	8.11	8.47	8.10	8.53	6.93	6.70
T********6026	11.50	11.07	13.54	12.20	11.98	12.76
T********5120	14.62	13.57	12.84	13.86	13.98	14.50
T********5318	16.21	14.07	11.12	10.12	9.87	8.78
T********7165	11.67	12.01	8.70	9.25	9.86	8.93
T********7850	11.06	12.63	11.93	12.10	11.20	12.05
T********3000	11.94	17.03	15.96	11.84	10.25	8.47
T********3389	6.39	10.37	8.12	8.96	9.87	10.04
T********5645	9.06	13.83	14.02	11.25	12.38	12.38
T********6282	7.86	12.99	10.36	10.67	12.53	11.75
T********1444	9.80	10.15	11.23	11.72	11.75	11.56
T********1769	10.07	10.03	9.34	8.76	7.83	8.19
T********1785	14.16	14.05	14.51	11.99	14.05	14.47
T********1799	10.59	11.05	11.26	10.28	10.81	10.53
T********9640	8.80	9.55	8.34	7.66	7.86	8.21
T********0303	9.87	8.70	8.97	9.27	9.67	9.49
T********2137	15.98	13.50	14.01	13.73	13.11	11.71
T********2576	10.41	11.30	10.45	10.90	9.87	9.70

Table 2.4
Color parameter, a* of 28 LR-ES measured during prolonged storage.

Sample Codes	D1	D42	D49	D56	D63	D70
T********8161	19.27	23.84	24.27	26.65	28.14	29.55
T********8164	14.98	18.54	19.78	22.09	25.85	27.90
T********8168	17.65	20.16	20.41	20.99	21.93	22.03
T********8169	17.61	19.97	19.98	22.12	22.16	22.62
T********6337	12.09	16.16	14.90	15.61	15.47	15.87
T********6346	12.80	16.51	16.51	18.86	17.78	18.57
T********6397	20.84	20.51	19.63	19.20	17.49	17.24
T********6402	18.63	20.88	21.19	23.07	21.78	23.23
T********3805	14.21	17.40	17.85	17.53	19.07	20.04
T********4693	16.25	18.13	18.76	18.63	20.27	20.35
T********4702	17.13	18.83	19.46	19.06	18.73	20.65
T********4703	20.29	23.27	23.91	25.52	28.78	28.56
T********3656	15.35	16.47	17.03	18.44	19.50	20.76
T********3661	15.45	18.49	19.65	22.30	23.38	26.77
T********3662	23.42	24.93	25.59	27.93	29.26	29.09
T********3664	17.72	21.73	22.49	25.25	27.75	29.69
T********8930	12.49	14.33	14.30	13.78	14.51	14.38
T********8933	15.84	19.38	19.47	19.72	19.95	21.55
T********8935	15.99	17.30	17.58	16.48	16.82	15.74
T********8938	15.45	16.82	16.43	16.28	17.25	17.62
T********5983	16.34	18.48	20.23	21.64	23.84	25.62
T********6163	18.49	19.09	20.53	22.23	22.96	24.59
T********6164	18.09	19.82	20.04	20.95	22.05	22.08
T********6184	22.14	22.76	24.59	24.68	26.53	25.33
T********0192	14.75	19.83	19.40	18.95	18.83	20.79
T********0423	19.36	20.81	22.13	21.71	21.12	21.77
T********0432	19.23	21.36	21.53	22.19	21.84	22.65
T********0433	13.36	16.81	17.20	17.41	17.38	18.51

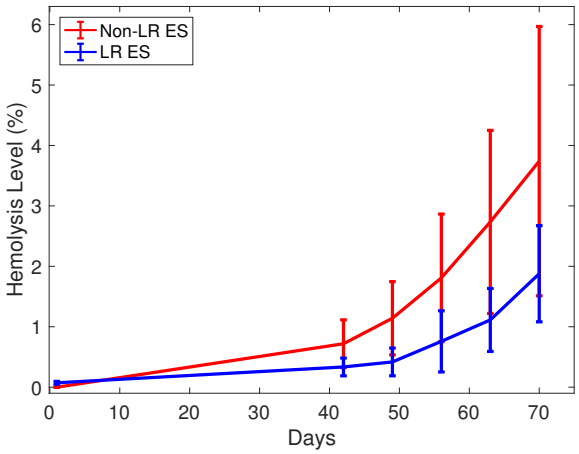

Figure 2.1 The increase in the hemolysis level of ES throughout the prolonged storage.

Diffuse reflectance spectra of samples were only collected for LR-ES. Average spectrum of whole samples exhibited alteration each week, as seen in Figure 2.2. Alterations were mainly observable after 600 nm and around 720 nm the reflectance values increased, while reflectance values decreased beyond the second local maximum point of the spectrum around 785 nm.

First derivative of the reflectance spectra with respect to wavelength were also investigated. Average of derivative spectra of samples in each week were plotted in Figure 2.3. Variations between weeks were higher between 600 nm and 850 nm.

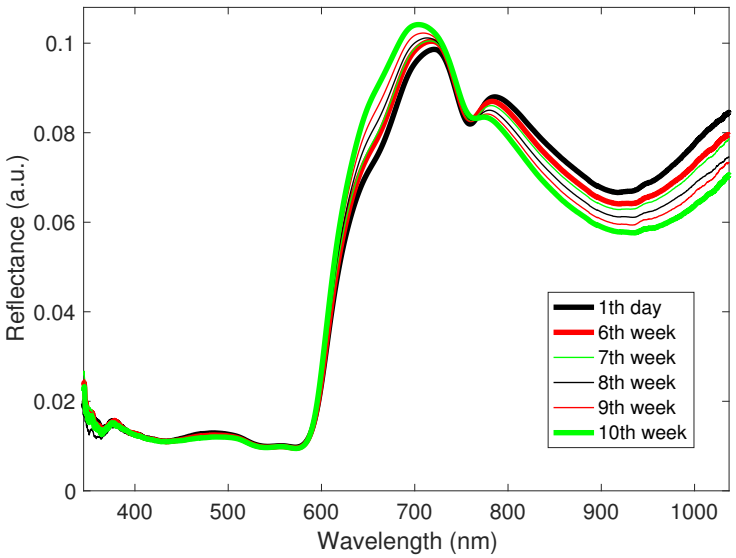

Figure 2.2 Alterations in diffuse reflectance spectra during prolonged storage.

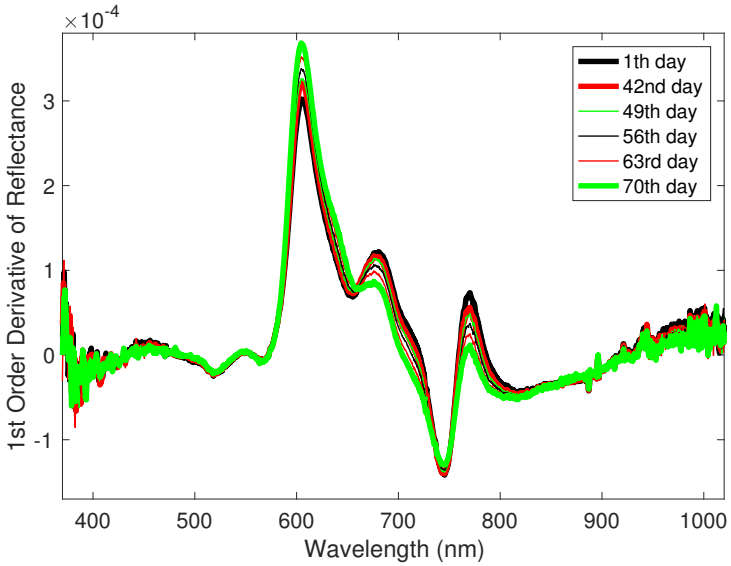

Figure 2.3 Alterations in derivative of diffuse reflectance spectra during prolonged storage.

2.4.2 Linear mixed model

The dependent variables of the model are from non-invasive reflection measurements, as it was assumed that the optical signal measured over the bag changed according to the physiological or hematological alterations. The dependent variables are the color coordinate values of CIELab: L*, a*, b*, chroma and hue-angle; the diffuse reflectance and the first derivative of diffuse reflectance spectrum at each wavelength. The independent variables of the model are chosen from the hematological variables. Since the main purpose of the study is to investigate blood quality associated parameters, FHB was selected as the independent variable in the first stage of the model. For the selection of sample specific independent predictors, the results of the repeated measures-ANOVA was utilized. Variables related to platelets and white blood cells were ignored in the model analysis. Variables affected by the storage period could not be used as the second level parameter; for this reason, only #RBC, THB and their interactions were added into the models, as between subject variables. All possible combinations of these variables were modeled and their statistical outputs were compared, according to the p-values of the estimates, total variances in the random errors and the percent reduction in variances (explained variances) due to addition of sample specific variables. Among thousands of models with different set of independent,

dependent and sample-specific variables, statistical outputs of the most accurate ones are listed in Table 2.5.

Since the reflectance data of NLR-ES were missing, only color parameters were examined as dependent variable (Model-1). Regarding to LR-ES, models with color parameters did not have statistically significant coefficients and the most accurate models using diffuse reflectance (Model-2) and derivative spectrum (Model-3) as dependent variable are presented in Table 2.5. Model-2 and Model-3 had better statistical outcomes, the p-values of estimated coefficients in these models were lower. The proportion of the explained variances in the between sample variances were also higher in Model-2 and Model-3. Although the variances in error terms were very distinctive, they could not be used to direct comparison, since they usually depend on the magnitude of the target variable. However, regarding p-values of estimated coefficients and the proportion of the explained variances, the derivative reflectance values seemed to fit better than other optical parameters in modeling the blood quality and hematology. Among time independent hematological variables, #RBC showed better relation with the optical data than THB.

2.5 Discussion

Two types of ES in blood bags were stored in standard storage conditions for 10 weeks in order to observe random effect of storage lesions on different ES. During the prolonged storage, the hematological variables and the non-invasive optical parameters were repeatedly measured. The outputs of the reflectance measurements were the color parameters in CIELab, diffuse reflectance values between 345 nm to 1037 nm, and the first derivative spectra of this diffuse reflectance spectra.

It was concluded that the relations between a* and hemolysis levels was non-linear, in contrast to the previous results [61]. Visual observations on blood samples with excessive FHB content agreed with this conclusion. Plasma of normal blood was in yellow color, when the hemolysis level was low, the extracellular medium of centrifuged

Table 2.5
Variables, estimates and statistical outputs of selected mixed models.

	Model-1 (NLR-ES- ES)		**Model-2 (LR-ES)**		**Model-3 (LR-ES)**	
Dependent Var.	hue-angle		R(λ=805.5nm)		dR(λ=902.5nm)	
Fixed Terms	**Coefficients**	**p-value**	**Coefficients**	**p-value**	**Coefficients**	**p-value**
Intercept	28.4824 (γ_{00})	<0.005	0.1241 (γ_{00})	<0.001	-4.52×10^{-7} (γ_{00})	<0.001
FHB(g/L)	11.8195 (γ_{10})	<0.05	-0.0553 (γ_{10})	<0.05	5.05×10^{-7} (γ_{10})	<0.005
THB(g/L)	-0.2840 (γ_{01})	0.1156				
$\#RBC$(1/L)			-6.30×10^{-15} (γ_{01})	<0.05	4.60×10^{-20} (γ_{01})	<0.001
$\#RBC$×FHB(g/L^2)	1.94×10^{-12} (γ_{11})	<0.05	7.63×10^{-15} (γ_{11})	<0.05	-7.88×10^{-20} (γ_{11})	<0.005
Random Terms	**Variances**	**Explained Var.**	**Variances**	**Explained Var.**	**Variances**	**Explained Var.**
$\mathbf{e_{ij}}$	1.2490		1.01×10^{-11}		1.04×10^{-32}	
$\mathbf{U_0}$	8.6519	19.05% (w/THB)	1.03×10^{-5}	17.52% (w/#RBC)	1.80×10^{-16}	39.26% (w/#RBC)
$\mathbf{U_1}$	2.6674	20.02% (w/#RBC)	1.88×10^{-5}	14.55% (w/#RBC)	7.73×10^{-12}	30.62% (w/RBC)

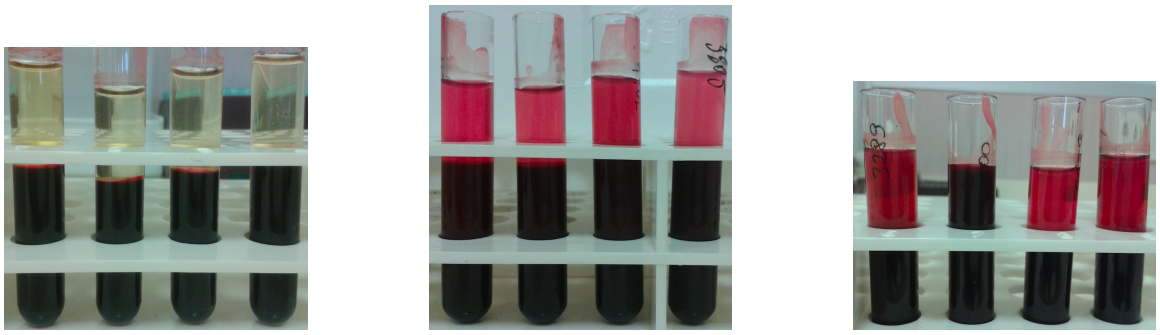

(a) (b) (c)

Figure 2.4 Illustrations of centrifuged ES having (a) no hemolysis, (b) mild hemolysis, (c) moderate hemolysis.

samples became pink tinged. However, in case of excessive hemolysis, the supernatant could not be distinguished visually from the cellular part after centrifugation. Color values of these samples measured with their digital images showed that the color value a* fell downward when the hemolysis index has become too high. This elucidates the measured color value a* of NLR-ES having excessive hemolysis levels (Table 2.3). Color values a* of LR-ES continued the increase throughout the 70 days storage (Table 2.4), because LR-ES did not have excessive hemolysis levels. The color value a* of LR-ES would decrease, if LR-ES had excessive hemolysis levels. Even though color parameter a* was clearly distinguish LR-ES or NLR-ES, mixed model suggested that reflectance and derivative of reflectance spectrum are better in modeling FHB concentration than the color parameters.

The reflectance values in the entire spectrum were used as dependent variable, but none of the spectral values wavelengths lead a notable model (Table 2.5). However, using derivation of the reflectance values brought some improvement in statistical outputs. Since the derivation means subtraction of two neighboring reflectance values, linear combination of multiple reflectance values may result in better estimates of FHB concentration.

Moreover, rather than linear mixed model, physically based models spanning concepts of light propagation in bag and blood; reflection portion of incident light due to absorption and reduced scattering coefficients of samples and bag would be more

accurate and appropriate.

Another consequence of this study was that there were sample specific variations affected by storage, which were MCV, RDW-SD, and RDW-CV. These variables may also affect the optical measurements and prevent us to establish the relationship between optical parameters and the blood quality. Besides, the hematological variables used as sample specific predictors did not fully explain the between-sample variations. Therefore, for the simplicity, optical reflectance parameters on the first day of the storage should have been investigated to model hematological variations. By this way, the blood quality parameter can be cancelled out, since it would be negligible in the first day of the storage.

3. EXPONENTIAL THEORY OF DIFFUSE REFLECTANCE IN MODELING HEMATOLOGICAL VARIABLES OF FRESH UNITS

3.1 Background and Objectives

The two common interactions of light with biological samples are scattering and absorption. In scattering (elastic scattering) phenomena, photons are deflected along new directions in the medium, but the energy (wavelength) of scattered photons remain unchanged. The absorption causes disappearance of the incident photons [66]. The wavelength-dependent reflectance from the bagged blood mostly contain elastically scattered and partially absorbed light. Therefore, the collected reflectance spectra are sensitive to their absorption and scattering coefficients, μ_a, μ_s, respectively. The asymmetry or anisotropy factor is also a fundamental optical property of a medium and defined as the average cosine of all scattering angles. It is usually denoted as g and takes values between -1 and 1. Positive values indicate a tendency of scattering to forward direction and negative values indicate backscattering. Isotroptic scattering stands for g=0.

These optical properties are unique parameters for the medium and their quantification is of the utmost importance for biomedical applications. The physical aspects of diffuse reflectance are reviewed in this Chapter and they are related with the optical properties of ES and the blood bag. The objectives are:

1. Introducing an analytical model of diffuse reflection from a two-layered, semi-infinite turbid medium, which representing ES in the blood bag.
2. Accounting for the first layer of two-layered media, measuring the optical properties of the blood bag with double integrating spheres.
3. Testing the model experimentally on fresh ES. The negligible hemolysis levels

of units were disregarded. Therefore, only the donor dependent hematological variations of ES were examined with diffuse reflectance measurements.

3.2 Diffuse Reflectance Theory

Light propagation in a turbid, both absorbing and scattering, medium is governed by radiative transport equation (RTE) [67]. In the basic form of this integro-differential equation, in a planar field, far from a light source, divergence of a radiance (L) to a direction $\hat{\boldsymbol{\omega}}$, at location $\mathbf{r}$ equals to weakened radiance due to total attenuation coefficient (μ_t) of the medium plus the integration of photon intensity scattered from all angles towards $\hat{\boldsymbol{\omega}}$ [68]:

$$\begin{aligned} \hat{\boldsymbol{\omega}} \cdot \nabla L(\lambda, \mathbf{r}, \hat{\boldsymbol{\omega}}) = & - L(\mu_t(\lambda), \lambda, \mathbf{r}, \hat{\boldsymbol{\omega}}) \\ & + \mu_s(\lambda) \int_{4\pi} L(\lambda, \mathbf{r}, \hat{\boldsymbol{\omega}}') P(\hat{\boldsymbol{\omega}}', \hat{\boldsymbol{\omega}}) d\hat{\boldsymbol{\omega}} \end{aligned} \tag{3.1}$$

The total attenuation coefficient μ_t is the sum of absorption and scattering coefficients and the term $P(\hat{\boldsymbol{\omega}}', \hat{\boldsymbol{\omega}})$ is the probability density function of radiation moving into a solid angle d$\hat{\boldsymbol{\omega}}$, for scattering into the direction $\hat{\boldsymbol{\omega}}$. This function is also called scattering phase function.

The RTE is usually solved either numerically [69] or by several analytical approximations [70], due to its complexity. Diffusion approximation is primarily used theory in the field of biomedical optics [71, 72, 73]. The main assumption of the diffusion approximation is that the scattering coefficient of the medium is much higher than its absorption coefficient and the radiance distribution in the medium is uniform [74]. Unfortunately, these assumptions are partially valid for blood samples. Absorption of blood is higher than or comparable to its scattering coefficient for the wavelengths below 600 nm [75]. Even though μ_s/μ_a becomes closer to 10^2 in the NIR region, diffusion approximation is still not applicable, since scattering inside blood is forward-directed and highly anisotropic (g>0.95) [75]. The other analytical estimates of RTE: dipole source model [76], photon migration model [77], path integral method [78] also use the

expressions of diffusion approximation and isotropic scattering phase functions.

Exponential model which was described by Zonios et. al. [79], however, offers a simpler expression of diffuse reflectance as a function of optical properties: absorption and reduced scattering coefficient (μ_s'), which is the portion of backscattered light and equals to $\mu_s \times (1-g)$. This model essentially ignores the integral term in the radiation transfer equation that represents the contribution of the scattered light intensity from all other directions to the direction of light propagation. Since blood tends to scatter light mostly in the forward direction and scattering angles are dominantly very low, it can be assumed that a pencil-beam of incident light would almost propagate in the same direction of the incident beam and it would be attenuated exponentially per unit path length. The second assumption of the exponential model is that the backscattered light is proportional to μ_s' of the medium and propagates in the opposite direction of the incident light [79].

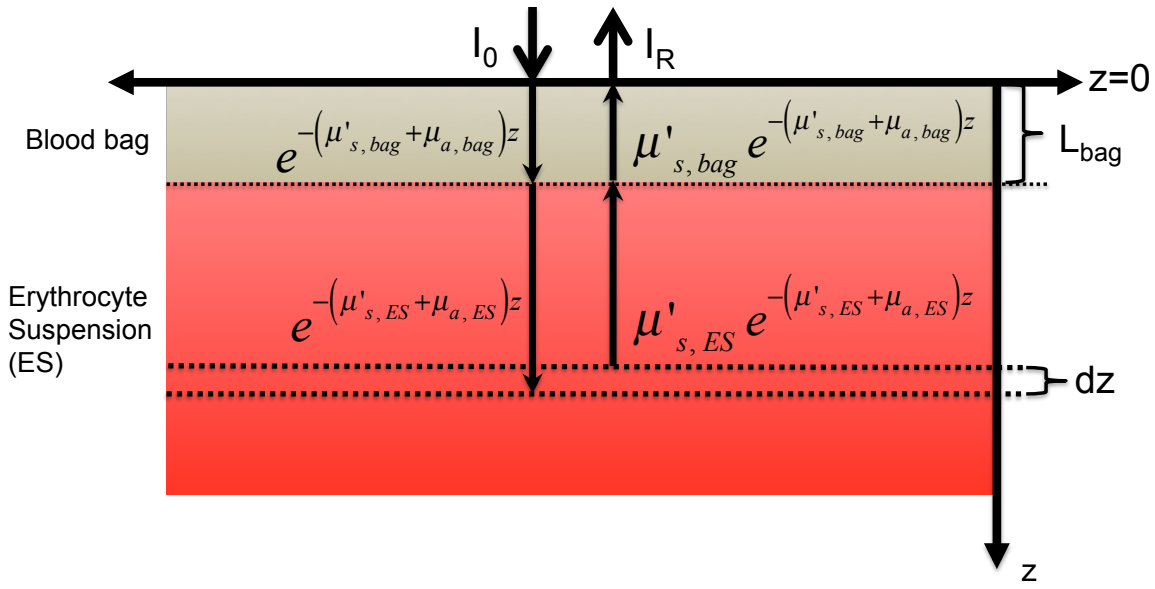

Figure 3.1 Illustration of the blood bag and ES as a two-layered, homogeneous, semi-infinite medium. The incident light with intensity I_0 is directed along the direction of z-axis and reflected back with intensity I_R. The arrows show the coefficient of the light attenuation along their length. $\mu_{a,bag}$ and $\mu'_{s,bag}$ are the absorption and reduced scattering coefficients of the bag and $\mu_{a,ES}$ and $\mu'_{s,ES}$ are the same parameters of ES, respectively. L_{bag} is the thickness of the bag. The intensity of the reflected light from an infinitesimally small layer dz is integrated from z=0 to infinite.

After these assumptions, the exponential model can be used to formulate the

total intensity of reflected light from a turbid medium. One-dimensional geometry of two-layered semi-infinite turbid medium, for the application of the bagged blood, is sketched as in Figure 3.1. The first layer is blood bag and the second layer is ES. The layers are assumed as optically homogeneous. The incident light (I_0) is first attenuated by the blood bag until z<L_{bag}, where L_{bag} is the thickness of the blood bag. Blood bag attenuates the light according to $\mu_{a,bag}$ and $\mu'_{s,bag}$. For convenience μ_s were used in replace of μ_s for each layers. In the ES, the light is further attenuated along the depth in the z-axis, according to $\mu_{a,ES}$ and $\mu'_{s,ES}$. Since the thickness of the ES is very large compared to L_{bag}, it is assumed to be infinite. The intensity of the cumulative reflected light I_R from an infinitesimally thin layer of dz is then [80]:

$$\begin{aligned} I_R =& I_0 \int_0^{L_{bag}} \mu'_{s,bag} e^{-2(\mu_{a,bag}+\mu'_{s,bag})z} dz \\ &+ I_0 e^{-2(\mu_{a,bag}+\mu'_{s,bag})z} \int_{L_{bag}}^{\infty} \mu'_{s,ES} e^{-2(\mu_{a,ES}+\mu'_{s,ES})z} dz \end{aligned} \tag{3.2}$$

Hence, the ratio of I_R to I_0 gives the diffuse reflectance (R_d) as:

$$\begin{aligned} R_d = \frac{I_R}{I_0} =& \frac{1}{2} \frac{\mu'_{s,bag}}{\mu'_{s,bag}+\mu_{a,bag}} (1 - e^{-2(\mu_{a,bag}+\mu'_{s,bag})L_{bag}}) \\ &+ \frac{1}{2} \frac{\mu'_{s,ES}}{\mu'_{s,ES}+\mu_{a,ES}} e^{-2(\mu_{a,ES}+\mu'_{s,ES}+\mu_{a,bag}+\mu'_{s,bag})L_{bag}} \end{aligned} \tag{3.3}$$

Note that the reflectance equation become much simpler when L $\to \infty$, in other words for one layer turbid media, the second term cancels out and the reflectance would be approximated to $\mu'_{s,bag}/(\mu'_{s,bag}+\mu_{a,bag})$. More interestingly, even for much thinner bags, the reflectance would be dominated by the optical characteristics of the first layer, if $\mu'_{s,bag}$ is very large. In all cases, diffuse reflectance would depend on at least one calibration parameter which corresponding optical properties of the bag.

The derived equation of diffuse reflectance (Eq. 3.3) actually counts for the total reflectance from the surface of the illuminated bag. However, in diffuse reflectance measurements, detectors can collect only a portion of this total reflectance. The measured reflectance depends on the geometry of the set-up. The diameter and collection efficiency of the detectors, source-detector and detector-sample distances are some of

the factors directly affecting the reflectance measurements. Additionally, there is refractive index mismatch between bag and blood since refractive index of the bag is about 1.5, while blood is around 1.34 - 1.37. The mismatch leads to multiple reflection of the light in the boundaries of the layers. The refractive index mismatches between bag and blood and even air-bag, detector-air interfaces should be considered in the formula for measured diffuse reflectance. With implementation of all these factors, as coefficients k_1, k_2, k_3 and k_4 into Eq. 3.3, the measured diffuse reflectance equation was simplified as:

$$R_m = k_1 + \frac{e^{k_2 + k_3 \mu_t}}{1 + k_4 \times \mu_{a,ES} / \mu'_{s,ES}} \tag{3.4}$$

The optical properties of the blood bag was replaced with the coefficient k_1. The power of the exponential term was written as a function of μ_t representing attenuations of both blood bag and ES. Other coefficients mostly correspond to the geometrical factors and the refractive index mismatch conditions.

3.3 Optical Properties of Erythrocyte Suspensions

Optical properties of ES may differ from those of blood in our circulation due to distinctive hematology of ES. In contrast to normal physiological blood, erythrocytes are densely packed in ES and HCT is around 50% to 70% [46]. Consequently, the #RBC and THB are higher in ES than whole blood. The count of red blood cells in ES is around 5.5 to 7.0 $\times$ 10^{12}/L and THB is in the range of 170 and 230 g/L, while MCHC is in the range of 320 and 360 g/L. After leukocyte filtration, the number of residual white blood cells is decreased below 10^6/L, while NLR-ES contain 10^{10}/L [81]. Filtration also reduces #PLT by ten fold, but their counts remain at the levels of 10^{10}/L for LR-ES [82]. The normal range of single erythrocyte volume is about 80 to 100 μm^3, but the size of the platelets are one tenth of the red blood cells. Since blood is collected from the veins of the donor, there would be non-oxygenated hemoglobin and the oxygen saturation levels of hemoglobin varies from 25% to 90% [83].

Absorption of blood is mainly dominated by red pigmented proteins, hemoglobin. More than 98% percent of the hemoglobin in blood exists in two main forms: unbounded hemoglobin (Hb) and oxygenated hemoglobin (Hb-O_2). These two types of hemoglobin have distinctive extinction coefficients especially after 600 nm (Figure 3.2). Their absorbance are very high in the lower wavelengths of the visible region compared to others blood components: platelets, plasma lipids and proteins, which also have absorption bands around these wavelengths [84]. However, in ES, these plasma constituents are removed and SAGM that has low absorbance only around NIR region region is added. As a result, $\mu_{a,ES}$ can be approximated with the concentrations of oxy- and deoxy- hemoglobin and hemoglobin oxygen saturation level ($SatO_2$), which is the fundamental parameter in calculating absorption coefficient of blood.

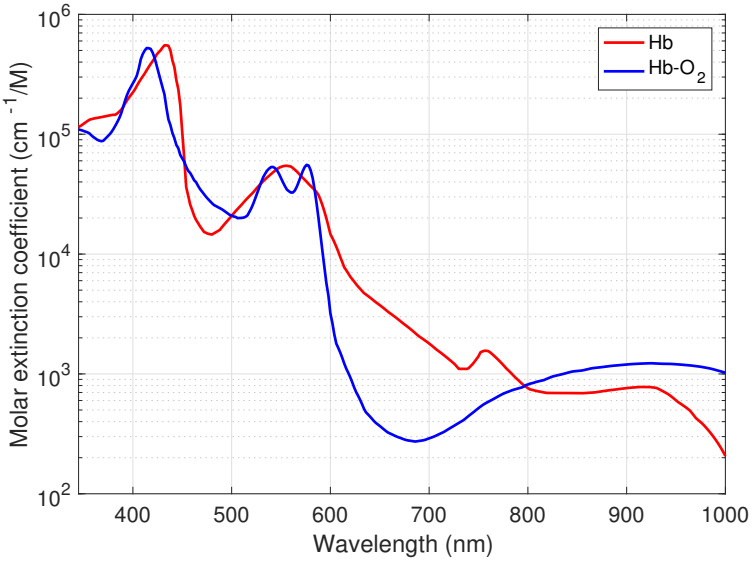

Figure 3.2 Molar extinction coefficient of oxy- and deoxy-hemoglobin (Hb-O_2, Hb). The data are available in Ref. [85].

In a solution that contains only distilled water and hemoglobin, the absorption coefficient would be proportional to the hemoglobin concentration. Unlike hemoglobin solutions, in normal blood, hemoglobin are densely distributed inside red blood cell membranes and only negligible hemoglobin concentration presents in the extracellular medium. Therefore, the most of the light is attenuated by this condensed hemoglobin in cells and it would be more precise to estimate the absorption coefficient of ES with

MCHC rather than THB. Hence, the absorption coefficient of ES is approximated as:

$$\mu_{a,ES} = MCHC \times [(\epsilon_{Hb-O_2} \times SatO_2 + \epsilon_{Hb} \times (1 - SatO_2)] \tag{3.5}$$

where $\epsilon_{\text{Hb-O}_2}$ and ϵ_{Hb} are the wavelength-dependent extinction coefficients of oxy-hemoglobin and deoxy-hemoglobin, respectively.

Scattering of light in ES is much complicated than the absorption. The red blood cells are the main contributors of light scattering [86]. According to Mie Theory, diameters, size ranges and volume densities of cells would determine the light scattering coefficient of ES [87]. Increasing of cell counts would increase the scattering coefficient, but for higher densities, the dependence become parabolic [88]. In fact, the refractive index mismatch between intracellular and extracellular media cause the light scattering from the cells [89]. Since the contents of extracellular medium would be same for each fresh ES, MCHC would be determinant of the scattering characteristics of ES.

In this study, the scattering coefficient of ES in Eq. 3.4 was replaced with the hematological variables: #RBC, MCV, RDW-CV, HCT, MCHC and Sat-O^2 and the results were compared.

3.4 Materials and Methods

3.4.1 Measurement of the optical properties of blood bag

Optical properties of the blood bag (Macopharma, Fr) was measured for investigating its contribution to diffuse reflectance data. Reflectance and transmittance of the blood bag were measured using double integrating spheres (Labsphere Inc.). In the measurement setup, an optical fiber, connected to the white light source (Ocean Optics, HL-2000), was directed to the entrance port of the first sphere through a lens and a diaphragm (Figure 3.3). The incident light beam was focused on the blood bag, which was placed between the spheres. Then, the reflected light and the transmitted

light were integrated in first and second spheres, respectively (Figure 3.3) and a fiber, connected to the detector ports of the spheres, transferred the integrated light into the spectrometer (Ocean Optics, USB4000-VIS-NIR). During the measurements, air inside the bag was discharged with a vacuum pump because air might form an additional layer between two plastic sheets and lead to errors in the measurements.

The measured reflectance and transmittance values were normalized with reference and dark measurements of both spheres. Finally, the inverse-adding-doubling (IAD) method was used to compute absorption and reduced scattering coefficients from the normalized reflectance and transmittance [91]. The IAD program was run three times for various estimated anisotropy factors of blood bag (g= 0.7, 0.8, and 0.9). The refractive index of the blood bag was assumed as 1.5. The IAD method requires additional inputs such as the dimensions of measurement geometry to calculate the optical properties. Other input values are listed in Table 3.1.

Table 3.1
Other inputs of IAD method for computing the optical properties of the blood bag [90].

Incident beam diameter	3.8 mm
Thickness(×2) of blood bag	0.66 mm
Diameter of spheres	83.8 mm
Diameter of the sample port of the spheres	12.7
Diameter of the entrance port of the first sphere	3.0
Diameter of the detector ports	0.2
Wall reflectance	99 %

3.4.2 ES samples

103 ES were used in these study: 87 of these units were LR and remaining 16 were NLR-ES. The units were gathered from 7 different blood bank centers. The preparation of LR-ES and NLR-ES are described in Section 2.2.1. Prepared units were rested at 4 ^{0}C for 24 hours, before the measurements.

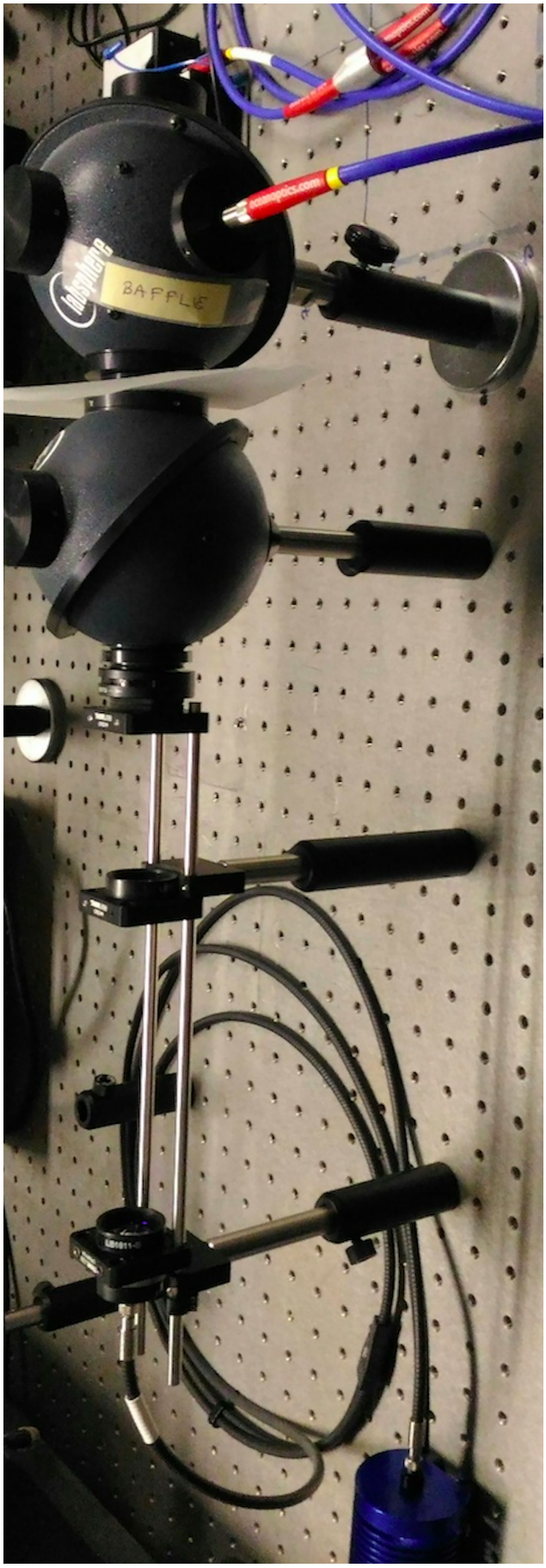

Figure 3.3 Set-up for total reflectance and total transmittance measurements of blood bag with double integrating spheres [90].

3.4.3 Diffuse reflectance measurements

Diffuse reflectance spectrum of the units were measured with a standard six-around-one reflection probe. The center fiber of the probe was used for illumination and the six fibers around the center one were used as detection of reflected light. The probe was placed in the 45^0 mount of the probe holder (Figure3.4). The bag laid on the board and the probe holder lightly squeezed it from the top. The light source, spectrometer and the software were as same as in Section 2.2.2.1.

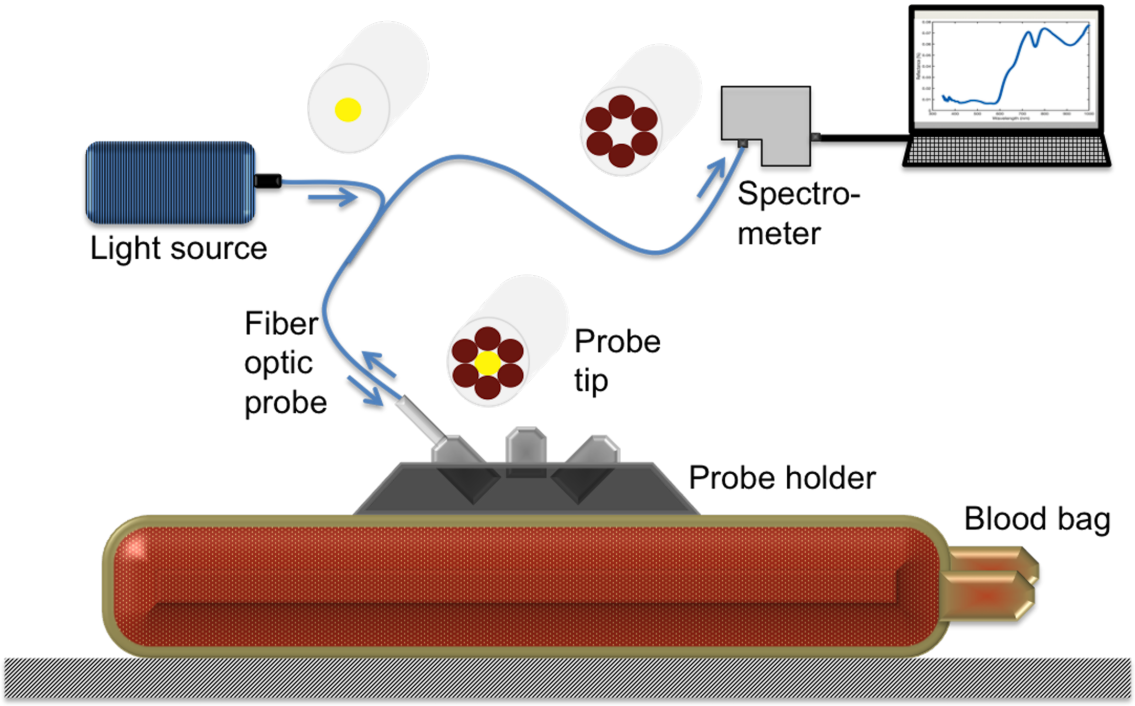

Figure 3.4 Illustration of the diffuse reflectance measurement of an ES [92].

3.4.4 Hematology analysis

Following the diffuse reflectance measurements, one tube of homogeneous blood sample was drawn from each bag and their hematological parameters were measured with automatic hematology analyzer (Mindray BC 3000 Plus). The device aspirates about 10 μl of blood from the tubes and dilutes it multiple times for enabling single

cell counting in a microchannel system. In this channel, passage of each cell through an aperture, where a constant electrical field is pre-existing, creates an electrical pulse proportional to cell size. The number of electrical pulses gives the number of cells and #RBC, #PLT and #WBC are determined from their known size ranges. The analyzer also plots histograms of each cell types and reads MCV, RDW-SD and RDW-CV.

The analyzer utilizes colorimetric method in measuring THB. A lysing solution that breaks membranes of erythrocytes and forms a hemoglobin solution mixed with the diluted sample, for colorimetric analysis. The absorbance of the hemoglobin solution at 525 nm yields THB. MCHC equals to the ratio of THB to HCT.

For the assessment of blood oxygen saturation level, $SatO_2$, the ratio of reflected light at two wavelengths: 760 nm and 790 nm was utilized [93]. Measuring oxygen saturation level with blood gas analyzer leads errors because time lapse between sample collection and analysis would increase the $SatO_2$ levels, when the samples are contaminated with air [94].

$$SatO_2(\%) = 150.60 \times \frac{R(\lambda = 760nm)}{R(\lambda = 790nm)} - 77.41 \tag{3.6}$$

3.4.5 Model analysis

Diffuse reflectance values at each wavelength were modeled with hematological variables of ES by using non-linear least squares regression based on the Eq. 3.4. $\mu_{a,ES}$ in Eq. 3.4 was replaced by the Eq. 3.5. For the replacement of the reduced scattering coefficient, hematological variables that are related to light scattering in ES were used. The hematological variables were compared by root mean squared error (RMSE) of the model in order to analyze their contribution to non-linear fit. In the power of the exponential term in Eq. 3.4, hematological variable as the counterpart of the $\mu_{s,ES}$ was omitted, and μ_t in equation 3.4 was considered as the summation of $\mu_{a,ES}$, $\mu_{a,bag}$ and $\mu_{s,bag}$ in the regression analysis. Matlab 2017 (Matworks Inc.) was used in all data analysis.

3.5 Results

3.5.1 Optical properties of the blood bag

As a result of the computational IAD method, $\mu_{a,bag}$ and $\mu'_{s,bag}$, between 400 and 1000 nm were obtained and plotted in Figure 3.5(a). Although there were noisy outputs in the side wavelengths, for the most of the wavelengths, both coefficients remained constant at the levels of 0.6 cm^{-1} and 7 cm^{-1}, respectively. The high noises at the side wavelengths were because of the low power of the halogen light source at these wavelengths. The inner surfaces of blood bags were generally modified to provide an appropriate contact with erythrocytes and minimize hemolysis (Figure A.7). These textures result in high scattering coefficients. In IAD, three different anisotropy factor were entered to observe its effect on the outcome, but as in Figure 3.5(b), it has no influence in computing $\mu_{a,bag}$ and $\mu'_{s,bag}$.

3.5.2 Hematological variations in ES units

Results of the hematology tests and estimations of $SatO_2$ of 103 ES were separately listed in the following table as NLR-ES and LR-ES. According to unpaired t-test, variables, except MCHC and MCV were significantly different for NLR-ES and LR-ES. These differences probably arose from the blood centers where the units were supplied. Factors in centrifugation: machine type, speed and time or variations in handling, filtration types such as top-and-bottom, top-and-top, could cause these variations.

3.5.3 Diffuse reflectance spectrum of ES

There was a strong negative correlation between estimated absorption coefficient with hematological variables according to Eq. 3.5, and diffuse reflectance spectra between 600 and 760 nm ($|r|>0.7$). The correlation coefficient reached -0.89 around 650 nm. Measured diffuse reflectance spectra of the units were in similar shape with

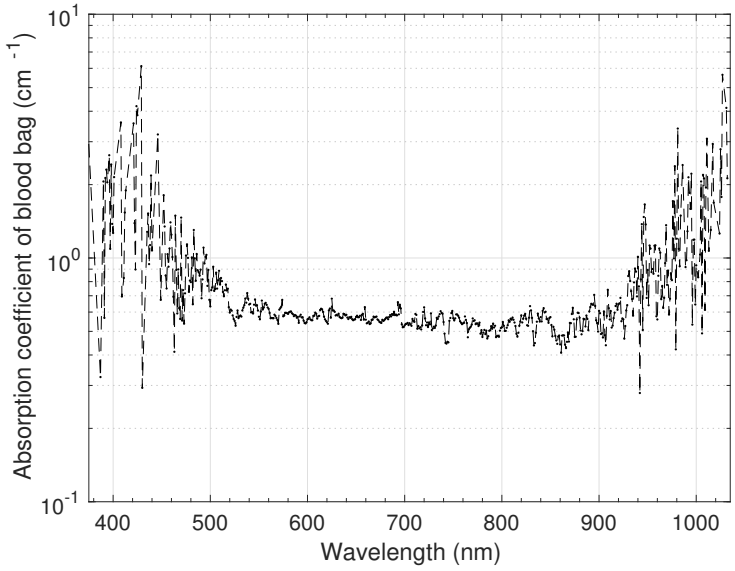

(a)

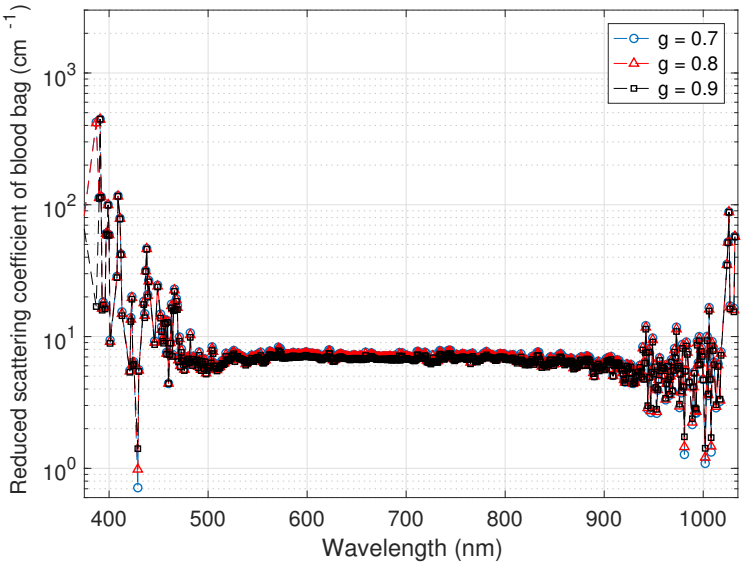

(b)

Figure 3.5 (a) Absorption and (b) reduced scattering coefficient of blood bag between 400 and 1000 nm.

the molar extinction coefficient of oxy-hemoglobin and deoxy-hemoglobin (Figure 3.6). A valley in a particular region of the diffuse reflectance spectrum corresponded to a peak molar extinction coefficient of hemoglobin at that wavelength. However, this inverse proportionality was broken in the 400 to 450-nm region where the absorption of hemoglobin molecules is highest, but it was not the region having lowest reflected light intensity, in diffuse reflectance spectrum illustrated in Figure 3.6. The diffuse re-

Table 3.2
Average values and ranges of measured hematological variables for NLR-ES and LR-ES, separately.

Hematological	**NLR-ES-ES (n=16)**			**LR-ES (n=87)**		
Variables	**Average**	**Min**	**Max**	**Average**	**Min**	**Max**
MCHC (g/L)	325 ±6	314	336	326 ±9	266	341
HCT (%)	63 ±4	56	69	59 ±2	52	67
#RBC (10^{10}/L)	686 ±42	588	732	650 ±43	559	892
#PLT (10^{10}/L)	27 ±12	6.3	49	1.6 ±0.3	0.9	2.3
#WBC (10^{10}/L)	1.0 ±0.2	0.6	1.4	NA		
MCV (μm^3)	92 ±4	83	100	91 ±5	70	104
RDW-CV (%)	15 ±1	14	18	14±1	12	22
Sat-O_2 (%)	55 ±8	43	72	56±11	35	82

flectance spectrum had a constant base level in the region where the $\mu_{a,ES}$ was higher. In this region, the detected light mostly contained the reflections from the blood bag.

There were high variety in diffuse reflectance spectra of ES units as seen in Figure 3.7. NLR-ES and LR-ES were plotted together in this figure, because there was not any significant difference between their reflectance spectra. Two distinctive spectra were clustering from others: one has higher reflectance distinctively between 800 and 1000 nm (green line) and the other one has the lowest reflectance between 700 and 800 nm (red line). These spectra correspond to ES units having lowest HCT and lowest MCHC, respectively. Additionally, the ES unit that was represented as red line in Figure 3.7(a) also contain highest #RBC, highest RDW-CV and lowest MCV (Table 3.2).

3.5.4 Non-linear least squares regression

Reflectance of ES units at 650 nm was used in the model analysis, because reflectance at 650 nm exhibited better correlation with $\mu_{a,ES}$. $\mu_{a,bag}$ and $\mu'_{s,bag}$ were also inserted in the model as 0.6 cm^{-1} and 7 cm^{-1}, respectively. Hence, the non-linear

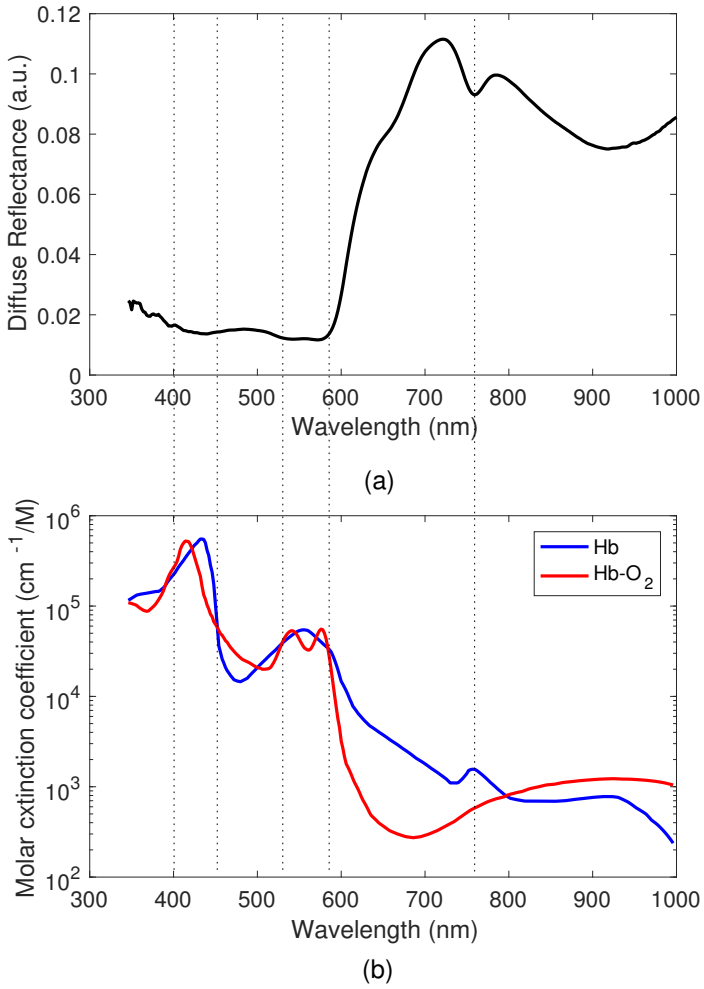

Figure 3.6 The similarity between (a) diffuse reflectance spectrum and (b) molar extinction coefficients of hemoglobin (Hb and Hb_{O_2}).

regression model turned into:

$$R_m(\lambda = 650) = k_1 + \frac{e^{(\mu_{a,ES}(\lambda=650)+7.6)\times k_3+k_4}}{1 + k_2 \times \mu_{a,ES}(\lambda = 650)/H} \tag{3.7}$$

where H corresponds to hematological variables replaced for the $\mu'_{s,ES}$ in Eq. 3.4.

First of all, a basic model was created. Vector of all ones was used for the variable H in Eq. 3.7. The basic model verified the assessment of $\mu_{a,ES}$ with hematological variables and the exponential theory as the diffuse reflectance model. The adjusted R^2 of the basic fit was computed as 0.8316 and RMSE was 0.0070.

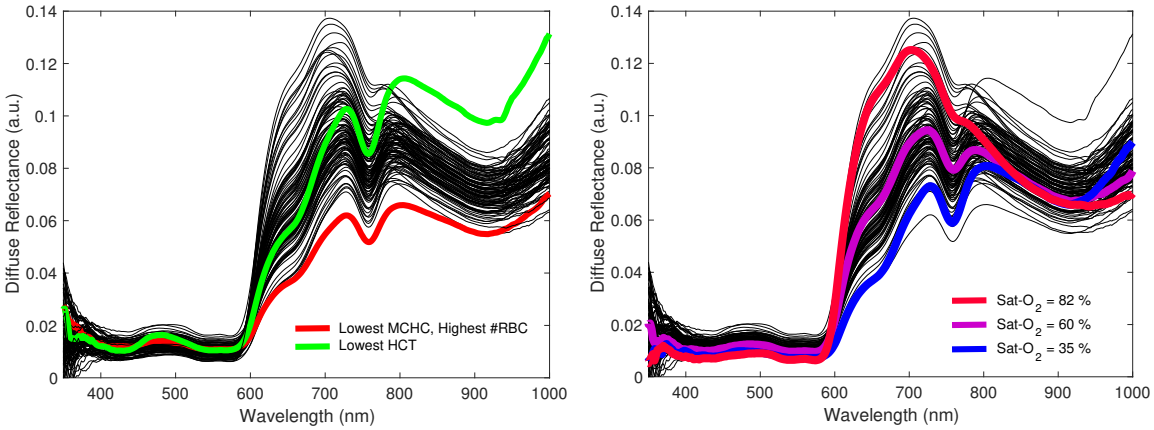

(a) (b)

Figure 3.7 Diffuse reflectance spectra of 103 samples: (a) clustering spectra due to extreme values in hematology, (b) the course of spectra according to oxygenation level.

Implementation of the other variables decreased RMSE, but their importance in the model were low compared to the importance of $\mu_{a,ES}$. Respectively, #RBC, MCV, HCT, RDW-CV provided better adjusted R^2 values: 0.8358, 0.8385, 0.8501, 0.8645. However, MCHC was the best for the variable H in Eq. 3.7; RMSE was reduced to 0.0053 and adjusted R^2 reached to 0.9057. When the model used for only 87 LR-ES, RMSE decreased to 0.0049 and adjusted R^2 became 0.9261. The nonlinear regression coefficients of the models with MCHC and their 95% confidence intervals were given in Table 3.3.

Table 3.3
The regression coefficients of the most accurate model, for LR-ES and for both types.

Reg.	**LR-ES (n=87)**		**Total (n=103)**	
Coef.	**Est.**	**CI (95%)**	**Est.**	**CI (95%)**
k_1	-0.25	(-0.41, -0.09)	-0.23	(-0.37, -0.09)
k_2	14.59	(3.55, 25.64)	18.36	(4.06, 32.66)
k_3	0.012	(0.007, 0.017)	0.014	(0.009, 0.019)
k_4	-0.82	(-1.08, -0.57)	-0.85	(-1.04, -0.65)

Three dimensional view of the non-linear regression model was illustrated in Figure 3.8. The accuracy of $\mu_{a,ES}$ in modeling R_m can be seen in the Figure 3.8(b).

NLR-ES were plotted blue color and they were distinguishable in the Figure 3.8(b). Excluding NLR-ES increased the model accuracy.

3.6 Discussion

In this Chapter, the exponential theory for light propagation in turbid medium was introduced. The exponential theory was examined in two-layered both absorbing and scattering media and the diffuse reflectance from such media, like blood in blood bag was derived from the exponential theory. The derived equation was further simplified by adding four calibration factors corresponding to measurement geometry, dimensions of the reflection probe and the optical properties of the blood bag. Instead of the optical properties of ES, their hematological counterparts were used. For instance, instead of using the actual value of $\mu_{a,ES}$, a function dependent to MCHC and Sat-O_2 was used (Eq. 3.5). Sat-O_2 was acquired from the ratio of the diffuse reflectance at 760 nm to 790 nm according to Ref. [93]. $\mu'_{s,ES}$ was substituted with the other hematological parameters. The optical properties of the blood bag were obtained by measuring total reflectance and total transmittance of the blood bag with double integrating spheres, then computing these outputs in IAD program. While $\mu_{a,bag}$ was around 0.6 cm^{-1}, which was expectable, $\mu'_{s,bag}$ found a bit higher (7 cm^{-1}). They were also inserted into the model. The model fitted better to data when MCHC was used as a replace of $\mu'_{s,ES}$ (R^2 reached to 0.93). MCHC may explain the light scattering in ES, because according to Mie Theory light scattering occurs due to the refractive index mismatches between the medium inside the particles (intracellular medium) and the surrounding medium (extracellular medium). MCHC of each ES would definitely vary the refractive index mismatch, so the light scattering coefficient, from sample to sample.

This study have shown that the hematological variations of individual ES could be modeled accurately and rather than statistical models such as mixed linear model, utilizing physically based models describing light propagation theory in turbid media was more adequate. Although the utilized exponential theory ignores the integral term

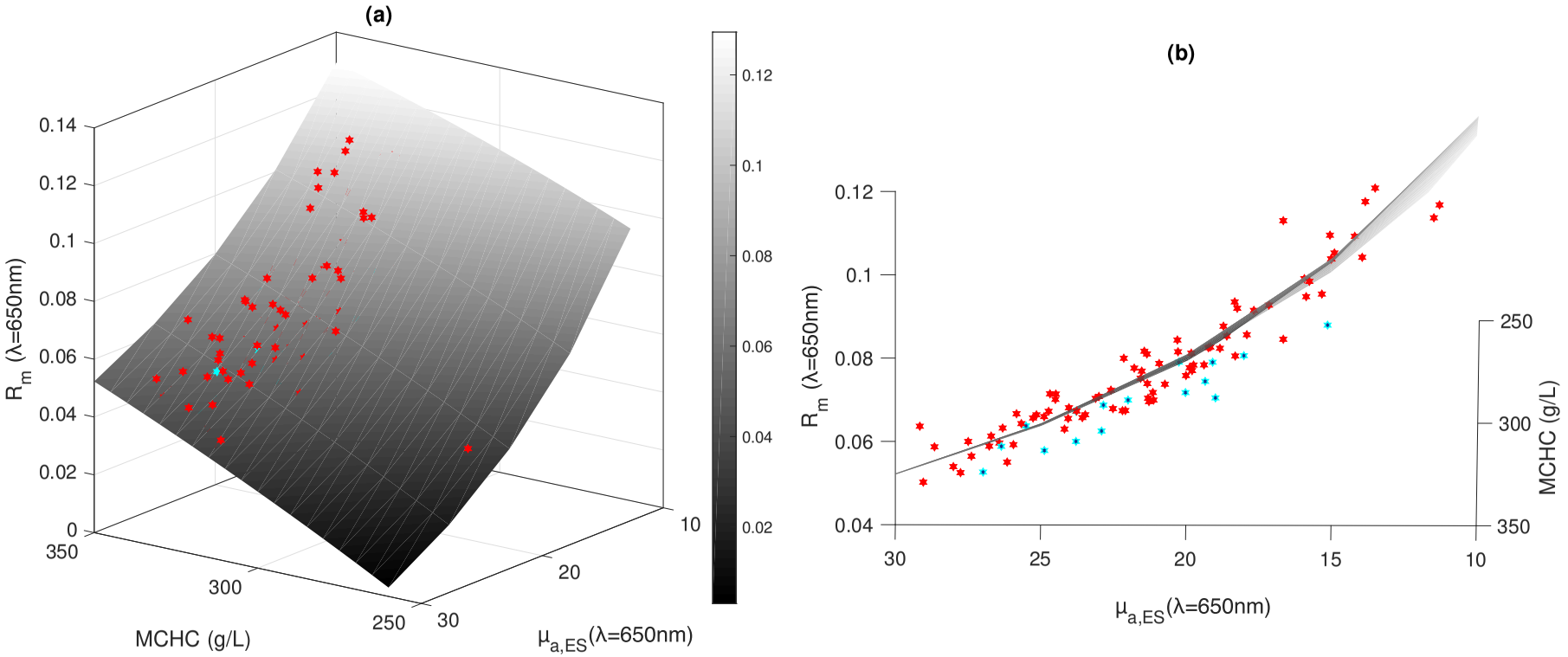

Figure 3.8 The non-linear fit to the data of ES in each types is illustrated in two different view: (a) top and (b) side. The blue markers represent the data of 16 NLR-ES and the red markers represent the data of 87 LR-ES.

in RTE, the final model fitted accurately with the experimental data collected from 103 ES units. Partitioning the units as LR-ES or NLR-ES increased the accuracy. Optical properties of the blood bag did not prevent evaluation of blood hematology; most of their influences were modeled inside regression coefficients.

Summarily, physically based exponential theory for diffuse reflectance model is sufficient for investigating physiological properties of blood non-invasively. However, the final equation is non-linear and it is supposed that the storage lesions more likely affect the scattering properties of ES than the absorption properties. For this reasons, for estimating blood quality parameter, more rigorous approximations of $\mu'_{s,ES}$ is needed.

4. SEMI-EMPIRICAL DIFFUSE REFLECTANCE EQUATION IN MODELING FREE HEMOGLOBIN CONCENTRATIONS

4.1 Introduction

The purpose of this Chapter is to introduce a simpler equation of reflectance for partitioning the effects of light scattering in blood, then creating a model to estimate FHB content in stored blood with non-invasive DRS.

4.2 Semi-empirical Diffuse Reflectance Equation

The exponential model introduced in the previous Chapter, expresses relation of reflectance and optical properties non-linearly. However, a semi-empirical equation, which first introduced by Zonios et. al. [95], allows conversion of diffuse reflectance equation as a linear function of optical properties μ_a and μ_s'. The model emphasizes on two fundamental facts that the reflected light from the sample is directly proportional to μ_s' and μ_a is inversely proportional to the reflected light intensity. Therefore, the diffuse reflectance in the semi-empirical equation is expressed as [79, 95]:

$$R_m = \frac{\mu_s'}{k_1 + k_2 \times \mu_a} \tag{4.1}$$

This equation was further developed in phantom studies [96, 97] with the motivation of its simplicity and ease of use in fiber-optic reflectance applications. The accuracy of the semi-empirical equation has been tested both with Monte Carlo simulations [95] and biological studies [96, 98, 99, 100, 101]. Its validity has been found adequate for a wide variety of turbid media having μ_a/μ_a between 0.1 and 1000 [79].

The semi-empirical equation was also tested in two-layered samples, but in fixed

conditions; (1) the refractive indices and reduced scattering coefficients of top and bottom layers were assigned with same value [102], and (2) the bottom layer was a non-absorbing layer [97]. However, in the case of bagged blood, both layers are turbid and have different optical properties and refractive indices. In this study, the optical properties μ_s' and μ_a' in Eq. 4.1 are presumed as the optical properties of ES units. For the optical properties of blood bag a new calibration factor was added in the semi-empirical equation. As it was previously observed, the diffuse reflectance never reached the zero-value even at wavelengths between 400 and 500 nm, where the hemoglobin absorption is highest. The reflectance actually remained at levels around 0.01 and 0.02. Therefore, a baseline reflectance is assumed to represent mostly optical properties of the blood bag. The semi-empirical equation in Eq. 4.1 for measured diffuse reflectance is modified accordingly:

$$R_m = k_1 + \frac{\mu'_{s,ES}}{k_2 + k_3 \times \mu_{a,ES}} \tag{4.2}$$

The empirical factors k_1, k_2 and k_3 are considered as the geometrical parameters, related to the measurement set-up and the fiber probe. However, k_1 is mostly dependent to reflectance from the bag and can be approximated as the lowest point in the diffuse reflectance spectrum.

4.3 Light Scattering in ES

Light scattering is physically diverging of the incident light when it encounter with particles. Light scattering depends on size of the particles, wavelength of the incident light and the refractive indices of the medium and the particles [87]. If the particles are in molecular level or the sizes are one tenth of the incident wavelength (i.e. smaller than 50 nm for visible light), Rayleigh scattering principles can be used to approximate the angular distribution of scattered light. However, micro-sized particles such as red cells or platelets comply with Mie Theory for light scattering [103]. Mie Theory can be used numerically calculate the scattering cross-section of a sphere particle in a suspension [104]. Although the red cells are in spheroid form, Mie Theory can

still be applied [105]. Since the Mie Theory describes single scattering from a cell, it works on solutions having very low concentration of particles. For defining scattering of highly concentrated particles, like ES, a correction factor is generally used [106].

The light scattering in ES can be described by the sum of densities of different cell types or particles and their scattering cross-section areas [107, 108, 109].

$$\mu_{s,ES} = \sum_{n} \frac{c_n}{V_n} \sigma_{s,n} \tag{4.3}$$

There are three types of main cells in blood and also particles inside extracellular medium. The quality associated FHB molecules also exist inside extracellular medium. The scattering coefficient of ES unit can be partitioned to its components as:

$$\mu_{s,ES} = \mu_{s,RBC} + \mu_{s,PLT} + \mu_{s,WBC} + \mu_{s,EXT} \tag{4.4}$$

$\mu_{s,EXT}$ represents the scattering coefficient, due to the particles in the extracellular medium. Scattering contributed by the platelets, $\mu_{s,PLT}$, for example, would be proportional to the ratio of platelet concentrations in ES to mean platelet volume (MPV):

$$\mu_{s,PLT} \propto \frac{PCT}{MPV} \tag{4.5}$$

Scattering coefficient of red blood cells is generally corrected with HCT-dependent factor [106, 108, 110, 111, 112, 113]. Number of authors were suggested different function for this correction factor: (1-HCT), (1-HCT)(1.4-HCT), $(1\text{-HCT})^2$ [75, 111, 113, 114].

$$\mu_{s,RBC} = \gamma(HCT) \frac{HCT}{MCV} \sigma_{s,RBC} \tag{4.6}$$

The scattering coefficient and scattering cross-sections in the above equations can directly be replaced by the reduced scattering coefficient and reduced scattering cross-sections due to the following equivalence:

$$\sigma_s' = \sigma_s \times (1 - g) \tag{4.7}$$

4.4 Effect of Storage on Optical Properties of Blood

During storage, erythrocytes undergo serious morphological and biochemical changes triggered by an inadequate ATP production due to slowing down of glycolysis reactions in the refrigerated conditions. The lack of ATP inactivates the sodium-potassium pumps, and potassium ions leave erythrocytes, while sodium and calcium ions accumulate inside. The ionic exchanges between the intracellular and extracellular media alter their refractive indices and light scattering from cells at the interface between cell membrane and the extracellular space. Although glycolysis reactions slow down in low temperatures, red cells continue to metabolize and the products of glycolysis make the media more acidic. The fall in pH reduces 2,3-DPG, which regulates binding of oxygen to hemoglobin and the hemoglobin oxygen affinity increases [115]. The hemoglobin oxygenation process changes the absorption characteristics of the ES unit. Free radicals derived from oxygenation cause red cell injury by damaging membrane phospholipids and cytoskeletal proteins. These oxidative damages and the loss of intracellular water and ions result in crenation of erythrocytes. Subsequently, the erythrocytes swell and form a sphere shape with multiple long spicules. These shape changes would definitely affect the scattering cross-section of red blood cells. Erythrocytes eventually loose these spicules as microvesicles into supernatant [35]. Microvesicles carry cytoplasmic particles from their originated cells. The size of the microvesicles range from 100 nm to 1 μm, and their concentration progressively increases during storage [116, 117]. The accumulation of these micro-sized membrane particles in supernatant would increase the number of scattering events in the extracellular medium. The decreasing surface-to-volume ratio of cells with the membrane fragmentation decreases the deformability, and oxidative damages to structural components of erythrocytes make them susceptible to hemolysis. Erythrocytes finally rupture and release cytoplasmic particles and hemoglobin into the cell suspending medium. This leads to an increase of scattering in the extracellular medium of ES.

4.5 Modeling the Free Hemoglobin Concentration

Storage lesions modify both $\mu_{a,ES}$ and $\mu_{s,ES}$ as described in Section 4.4. However, the FHB concentration, which is a substantial element for quality assessment of blood products, is expected to be in correlation with the increase of scattering from the extracellular medium. The combined effect of storage lesions on the overall $\mu'_{s,ES}$ is unpredictable, but accumulation of microvesicles, cellular particles, and the FHB into the extracellular medium would increase the contribution of scattering from the extracellular medium. For investigating $\mu'_{s,EXT}$, Eq. (1) is rewritten as:

$$\mu'_{s,ES} = k_2[R_m - k_1]\mu_{a,ES} + k_3[R_m - k_1] \tag{4.8}$$

In order to reduce the number of parameters, the normalized reflectance is used instead of R_m. Diffuse reflectance values at each wavelength are normalized by measured reflectance at 570 nm, where the diffuse reflectance spectra have minimum value.

$$R_{norm}(\lambda) = R_m(\lambda) - R_m(\lambda = 570nm) \tag{4.9}$$

After partitioning $\mu'_{s,ES}$ as in Eq. 4.4 and omitting $\mu'_{s,WBC}$, $\mu'_{s,EXT}$ can be expressed as:

$$\mu'_{s,EXT} = k_2[R_m - k_1]\mu_{a,ES} + k_3[R_m - k_1] - \mu'_{s,RBC} - \mu'_{s,PLT} \tag{4.10}$$

Since the FHB concentration is associated with the increase in $\mu'_{s,EXT}$, Eq. 4.10 can be used to model the FHB concentration. After substituting, $\mu_{a,ES}$, $\mu_{s',RBC}$, and $\mu'_{s,PLT}$, according to Eq. 3.5, 4.6 and 4.5, respectively, the FHB concentration can be modeled with regressors depending on only the diffuse reflectance and the hematological parameters. Immeasurable covariates such as scattering cross-sections and anisotropy factor can be covered by the regression coefficients. The details and results of modeling are given in Section 4.6.4 and 4.7.2.

4.6 Methodology

4.6.1 Monte Carlo simulations

Effects of the optical properties of ES on the intensity of diffuse reflected light were simulated with the Monte Carlo multilayer code [118]. Three layers were structured for ES units; the first and the last layers were the blood bag (thicknesses of 0.03 cm) and ES the mid-layer thickness 1.54 cm. The simulation was run 196 times, for 14 $\mu_{a,ES}$, logarithmically increasing from 1 to 3000 cm^{-1}, and 14 $\mu_{s,ES}$ ranged from 250 to 900 cm^{-1}, in 50 cm^{-1} increments. $\mu_{a,bag}$ was set to 0.6 cm^{-1} and $\mu_{s,bag}$ assigned as 35 cm^{-1}. The anisotropy factor of the bag was set to 0.8, and $\mu'_{s,bag}$ became 7 cm^{-1}. The refractive index and anisotropy factor of ES ware assumed to be 1.37 and 0.95, respectively. The Henvey-Greenstein phase function was used for the random scattering process. 10^6 photons were launched in each run, oblique angle was defined to incident beam as 45^0 degree relative to the normal of blood bag surface, in order to reduce escaping of photons from the last layer. The total diffuse reflectance was considered for analysis. Gradient of total diffuse reflectance with respect to the reduced scattering and absorption coefficients were recorded and the accuracy of the semi-empirical equation was analyzed.

4.6.2 Measurement of the calibration factors

Following the simulations, validation of the proposed semi-empirical equation Eq. 4.1 was trained on phantoms. The calibration factors k_1, k_2 and k_3 which depend on the measurement geometry and optical properties of the blood bag, were computed.

Liquid optical phantoms were prepared by mixing black Indian ink and Intralipid®. The black ink has two absorption bands below 600 nm and very low or zero absorption after 700 nm, similar to hemoglobin. Intralipid® acts like blood cells, due to the contents of micro-sized hydrophobic fat droplets. Detailed information about the optical properties of Indian ink and Intralipid® and phantom studies are given in

the Appendix.

First, 7 phantoms each having 3, 4.5, 6, 7.5, 9, 10.5 and 12 ml of Intralipid®-20%, respectively were prepared. Distilled water was used as the host medium. The total volume of each phantoms was 150 ml. They were funneled into 7 separate pediatric blood bags (Kansuk, Turkey). After measuring the diffuse reflectance of the set of 7 phantoms, concentration of Indian ink in the bags were gradually increased. Sampling rate of absorption coefficient was kept this much for obtaining accurate calibration factors representing optical properties in wider range. Diffuse reflectance of each phantom was measured as described in Section 2.2.2.1.

4.6.3 Measuring data of ES units

40 LR-ES were used in this study; the model was built with the 28 of them and the validation tests were made on the remaining units. Diffuse reflectance measurements and hematology analysis were performed as described in Section 2.2.2.1 and 2.2.2.2. Reference FHB measurements and the calculation of hemolysis degree was performed as described in Section 2.2.2.3.

4.6.4 Generalized linear model (GLM) for predicting the FHB concentration

The GLM was used to relate the FHB concentration with the reduced scattering coefficient of extracellular medium. The general expression of GLM is of the form:

$$\mathbf{X} \cdot \mathbf{b} + \mathbf{e} = \mathbf{Y} \tag{4.11}$$

where $\mathbf{X}$ is the design matrix and $\mathbf{b}$, $\mathbf{e}$, and $\mathbf{Y}$ are the vectors of regression coefficients, residuals, and outcome variable, respectively. The design matrix is composed of predictors ($\mathbf{X}_{\mathrm{p}}$). Diffuse reflectance and hematological variables were used as predictors, and formatted according to 4.10, with the expressed $\mu'_{s,EXT}$, replaced by the FHB con-

centration, as the outcome variable of the model. At a given wavelength λ, the matrix representation of GLM is:

$$\begin{bmatrix} X_1^{1,1} & X_2^{1,1} & \cdots & X_p^{1,1} \\ \vdots & \vdots & & \vdots \\ X_1^{1,j} & X_2^{1,j} & & X_p^{1,i} \\ X_1^{2,1} & X_2^{2,1} & & X_p^{2,1} \\ \vdots & \vdots & & \vdots \\ \vdots & \vdots & & \vdots \\ X_1^{i,j} & X_2^{i,j} & \cdots & X_p^{i,j} \end{bmatrix}^{(\lambda)}_{(i\times j)\times p} \begin{bmatrix} b_1 \\ b_2 \\ \vdots \\ b_p \end{bmatrix}^{(\lambda)}_{p\times 1} + \begin{bmatrix} e_{1,1} \\ \vdots \\ e_{1,j} \\ e_{2,1} \\ \vdots \\ \vdots \\ e_{i,j} \end{bmatrix}^{(\lambda)}_{(i\times j)\times 1} = \begin{bmatrix} Y_{1,1} \\ \vdots \\ Y_{1,j} \\ Y_{2,1} \\ \vdots \\ \vdots \\ Y_{i,j} \end{bmatrix}_{(i\times j)\times 1} \tag{4.12}$$

Indices p, i, and j represent the number of predictors, the number of repeated measurements, and the number of ES units during storage, respectively. The GLM was applied 328 from 344 to 1000 nm, with 2-nm increments. The GLM of each wavelength was analyzed according to their goodness of fits, RMSE, and statistical significance of their regression coefficients. Best models fitting the training set and the models having better predicting ability for the data in the validation set are demonstrated. Matlab 2017b (Mathworks Inc.) was used for statistical analysis.

4.7 Results

4.7.1 Validity of the semi-empirical equation

The semi-empirical equation was tested with Monte Carlo simulations. The exponential model and the proposed semi-empirical equation fitted to 196 simulation results, as seen in Figure 4.1. Since the range of the absorption coefficient was very large, models did not fit the whole data. Then the data was separated into two parts; for low ($\mu_{a,ES} \leq$100 cm^{-1}) and high $\mu_{a,ES}$ (100 cm^{-1}$< \mu_{a,ES} \leq$3000 cm^{-1}). For the low absorption levels, the exponential model fitted perfectly (R^2=0.999) (Figure 4.1(a)). Nevertheless, the fitness of the semi-empirical equation to simulations was also acceptable (R^2=0.929), for low $\mu_{a,ES}$ (Figure 4.1(a)). For $\mu_{a,ES}$ <5 cm^{-1}, the relationship

between the reduced scattering coefficient and the diffuse reflectance has become non-linear and the deviations of simulation results from semi-empirical equation increased, but the exponential model fitted accurately. At very high absorption levels of ES, the goodness of fit of the semi-empirical equation has reached to 0.992 (Figure 4.1(b)). The results support the idea that, the total diffuse reflectance converged to k_1, for high absorption levels.

Besides simulations, phantom studies were performed to investigate the validity of the semi-empirical equation in relating the reflectance of two-layered turbid samples. Calibration factors were computed by using the non-linear least squares curve fitting procedure. The goodness of fit was above 0.995 for most of the spectrum. The calibration factor k_1 was found as a basal reflectance for the entire spectrum, as it was presumed. k_2 was inversely proportional to the wavelength and $\lambda^{-1.74}$ fits well with the curve in Figure 4.7.1. There was a small fall between 400 and 500 nm in the calibration factor, k_3.

4.7.2 Results of GLM for FHB prediction

For estimating the response variable FHB concentration, the selected predictors of GLM are:

$$
\begin{aligned}
X_1 &= 1 \\
X_2(\lambda) &= R_{norm}(\lambda) \times \frac{1}{1 - HCT} \\
X_3(\lambda) &= R_{norm}(\lambda) \times MCHC \times SatO_2 \times \epsilon_{Hb-O_2}(\lambda) \times \frac{1}{1 - HCT} \\
X_4(\lambda) &= R_{norm}(\lambda) \times MCHC \times (1 - SatO_2) \times \epsilon_{Hb}(\lambda) \times \frac{1}{1 - HCT} \\
X_5 &= \frac{HCT}{MCV} \\
X_6 &= \frac{HCT^2}{MCV} \\
X_7 &= \frac{PCT}{MPV} \times \frac{1}{1 - HCT}
\end{aligned}
\tag{4.13}
$$

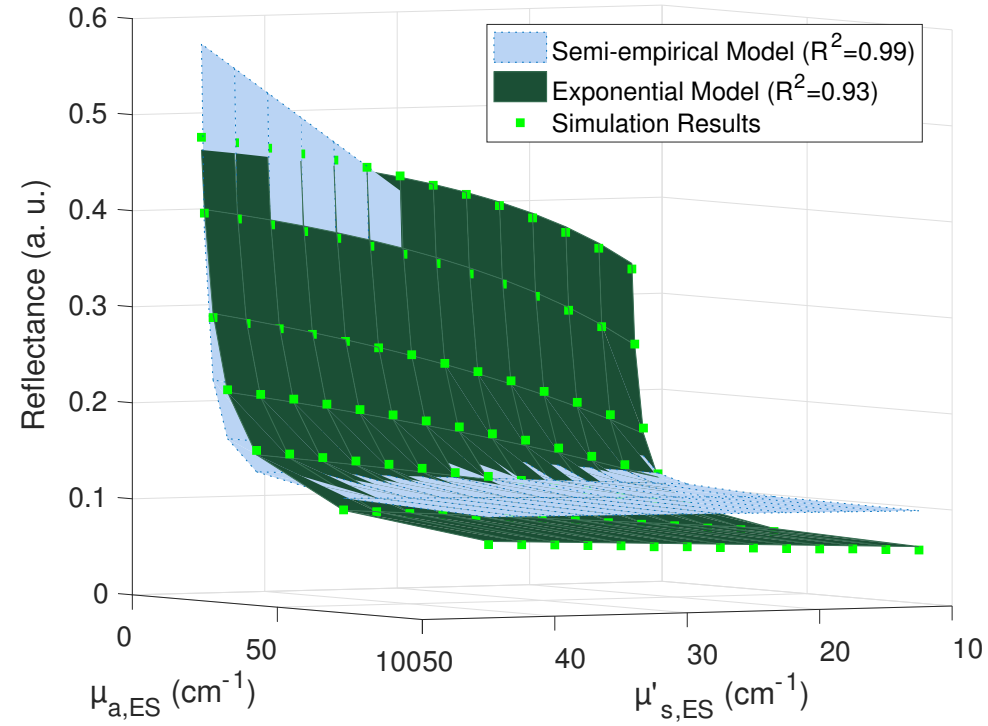

(a)

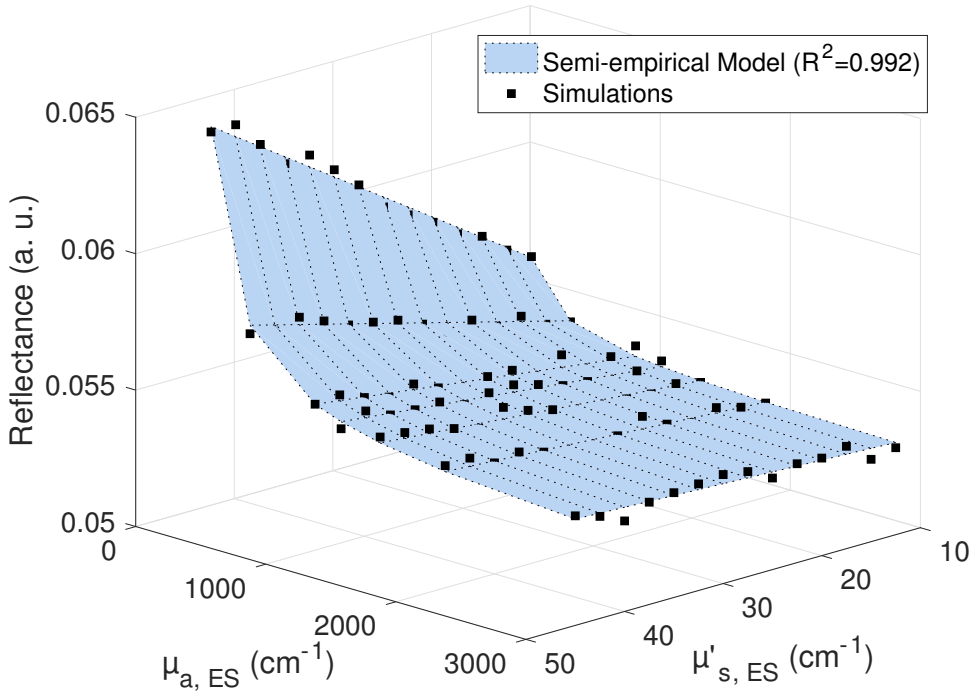

(b)

Figure 4.1 3-D plots of the results of Monte Carlo simulations: (a) for low absorption coefficients of ES ($\mu_{a,ES} < 100cm^{-1}$) and for higher absorption coefficients of ES. x and y axes are $\mu'_{s,ES}$ and $\mu_{a,ES}$ and z axis represents the reflectance values obtained from the simulation results.

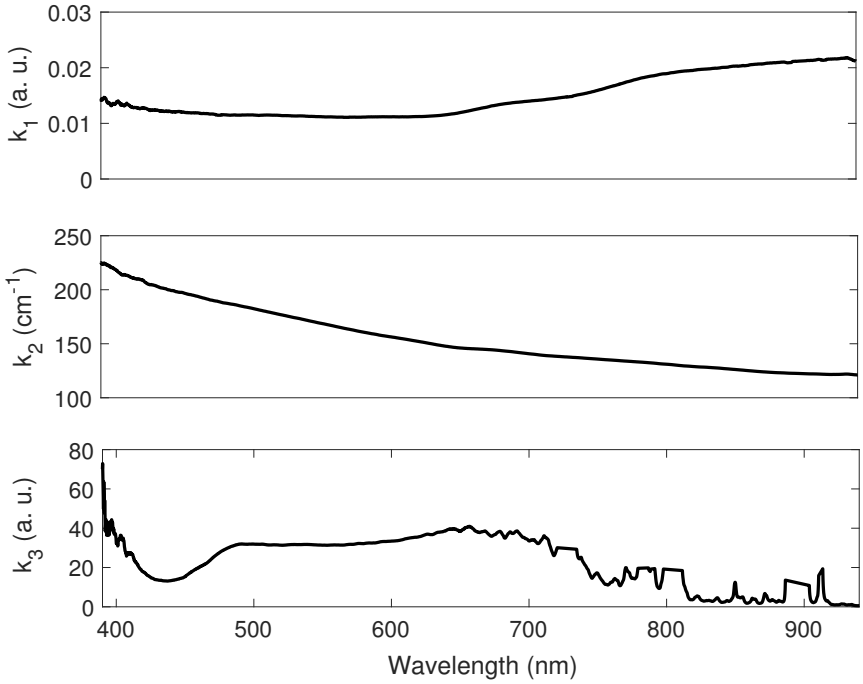

Figure 4.2 Spectral illustration of the calibration factors: k_1, k_2, and k_3.

where X_1 represents the intercept vector of GLM. X_2 includes normalized diffuse reflectance, described in Section 4.5. Absorption of oxy-hemoglobin and deoxy-hemoglobin were separated into two predictors, X_3 and X_4. $\mu'_{s,RBC}$ in Eq. 4.10 was replaced according to Eq. 4.6. The HCT-dependent empirical factor, $\gamma(HCT)$, mentioned in Section 4.3, was assumed to have the form (1-HCT)^2 or (1-HCT)(1.4-HCT). The polynomial terms of $\mu'_{s,RBC}$ were split into two predictors X_5 and X_6. X_7 was used as the replacement of $\mu'_{s,PLT}$ in Eq. 4.10. All predictors are divided by (1-HCT), i.e., the concentration of extracellular medium. It is cancelled out by the same factor of $\gamma(HCT)$ for predictors X_5 and X_6.

The GLM below 770 nm gave statistically significant regression coefficients ($p<0.05$). The significance of the regression coefficients is shown in Table 4.1 by their ranges of p-values through the wavelengths. The correlation coefficients between the reference and predicted FHB concentration ranged from 0.80 to 0.85 and the RMSE were between 2.45 and 2.75 g/L for the GLM of wavelengths in the visible spectrum. The goodness of fits of the models was in a similar range ($0.64<R^2<0.71$) for all models. It was also observed that no particular wavelength had a priority for estimating FHB concentration.

Table 4.1
p-values of the regression coefficient for the models using the reflectance in the visible spectrum.

Regression Coef.	p-value ranges (370-770 nm)	average of p-values in the range
$b_1(\lambda)$	$\sim 10^{-5}$ - 0.027	0.0044
$b_2(\lambda)$	$\sim 10^{-11}$ - 0.048	0.0053
$b_3(\lambda)$	$\sim 10^{-10}$ - 0.033	0.0011
$b_4(\lambda)$	$\sim 10^{-14}$ - 0.017	$\sim 10^{-5}$
$b_5(\lambda)$	$\sim 10^{-14}$ - $\sim 10^{-5}$	$\sim 10^{-6}$
$b_6(\lambda)$	$\sim 10^{-16}$ - $\sim 10^{-5}$	$\sim 10^{-6}$
$b_7(\lambda)$	$\sim 10^{-4}$ - 0.011	0.033

The ratio of the regression coefficients b_5 to b_6 informed us about the $\gamma(HCT)$, because b_5 and b_6 are both related to $\mu'_{s,ES}$. This ratio was expected to be around -1 or -1.4, for being consistent with the suggested empirical factors in the literature. For most of the spectrum, the ratio was calculated around -1 (Figure 4.3(a)). Second, the ratio of the regression coefficients b_3 and b_4 were expected to be proportional to the ratio of molar extinction coefficients of oxy- and deoxy-hemoglobin because molar extinction coefficients were sample independent factors and their magnitude would merge into regression coefficients. The ratio, plotted in Figure 4.3(b), confirms this assumption.

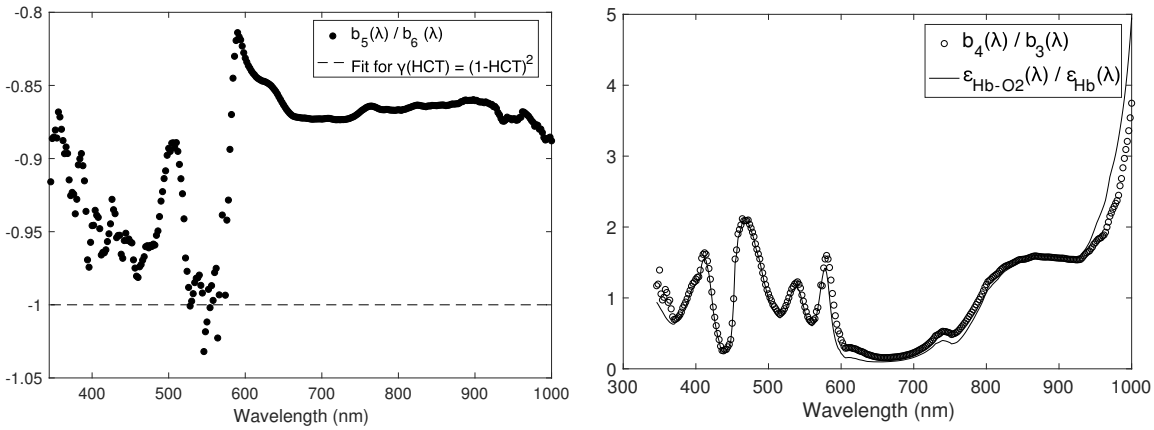

(a) (b)

Figure 4.3 Spectral illustration for the ratio of the regression coefficients: (a) b_5/b_6 and (b) b_4/b_3.

4.7.3 Accuracy of GLM on validation set

The FHB concentrations of the ES units in the validation set were predicted with the regression coefficients computed from the training set. The predictions were compared with the actual FHB concentrations. Maximum goodness of linear fit, was read 0.81, and the correlation coefficient between reference and predicted FHB concentrations were 0.90. Minimum RMSE was computed as 1.32 g/L.

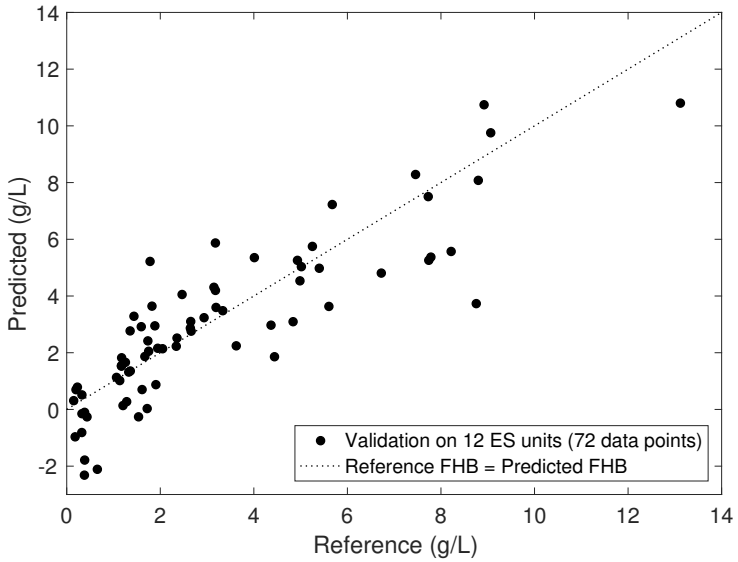

Figure 4.4 Predicted versus reference FHB concentrations, with GLM, using reflectance at 518 nm. The goodness of fit is 0.75.

Although predicting the exact value of FHB concentration could not be achieved with the proposed model, the model predicted and actual FHB concentrations were highly correlated, suggesting that the model can give accurate information about the quality of the blood under storage. Since it is the quality indicator, the hemolysis levels of ES units were calculated from the following equation after predicting FHB concentrations with the proposed model:

$$Hemolysis\,level\% = \frac{FHB}{MCHC} \times \frac{1 - HCT}{HCT} \times 100 \tag{4.14}$$

The ES units having hemolysis levels higher than the limit levels were judged as low quality units. The true condition was compared with the assignments according to these predictions. For the threshold of 0.8% hemolysis, the maximum accuracy was observed

as 63/72 (∼88%) for the model using reflectance at 518 nm. For the threshold of 1.0% hemolysis, the maximum accuracy was observed as 66/72 (∼92%) for the model using data at 544 nm. According to the confusion matrix of these two models (Figure 4.5), sensitivity and specificity of the former was calculated as 81% and 90%, respectively. In the latter, estimating true negative ratio increased to 52/54 making specificity ∼96%, but meantime the sensitivity fell to 78%.

4.8 Discussion

A modified version of semi-empirical reflectance model was proposed for extracting quality information of stored blood. There were limited number of researches in the literature, for the application of semi-empirical equation on multi-layered turbid samples [97, 102]. In this study, the measured diffuse reflectance was directly related to the reduced scattering and the absorption coefficient of the second layer. The approach was validated with both Monte Carlo simulations and measuring phantoms with predefined optical properties. Calibration factors were computed with very high accuracy and for the simulation, results were very similar to those of the physically based exponential model described in Chapter 3. In contrast to the exponential model, the diffuse reflectance is linearly dependent on the reduced scattering coefficient of ES in the semi-empirical equation. This property enabled us modeling the effect of FHB concentration on the light scattering trends of the stored blood. There are multiple factors affecting the optical properties of blood and only few of them are quality associated. The influence of storage lesions on the scattering and the absorption coefficients is chaotic and direction of the overall effect is unpredictable. For this reason, monitoring timely changes of the scattering or the absorption coefficients alone would not be informative about blood quality. It is proposed that the accumulation of cytoplasmic particles, FHB molecules and microvesicles would increase the number of light scattering events in the extracellular medium. With this assumption, the scattering coefficient of ES unit was divided into its components. A linear model constructed to uncover the relatively small effects of extracellular particles and platelets on light scattering, compared to scattering by red cells.

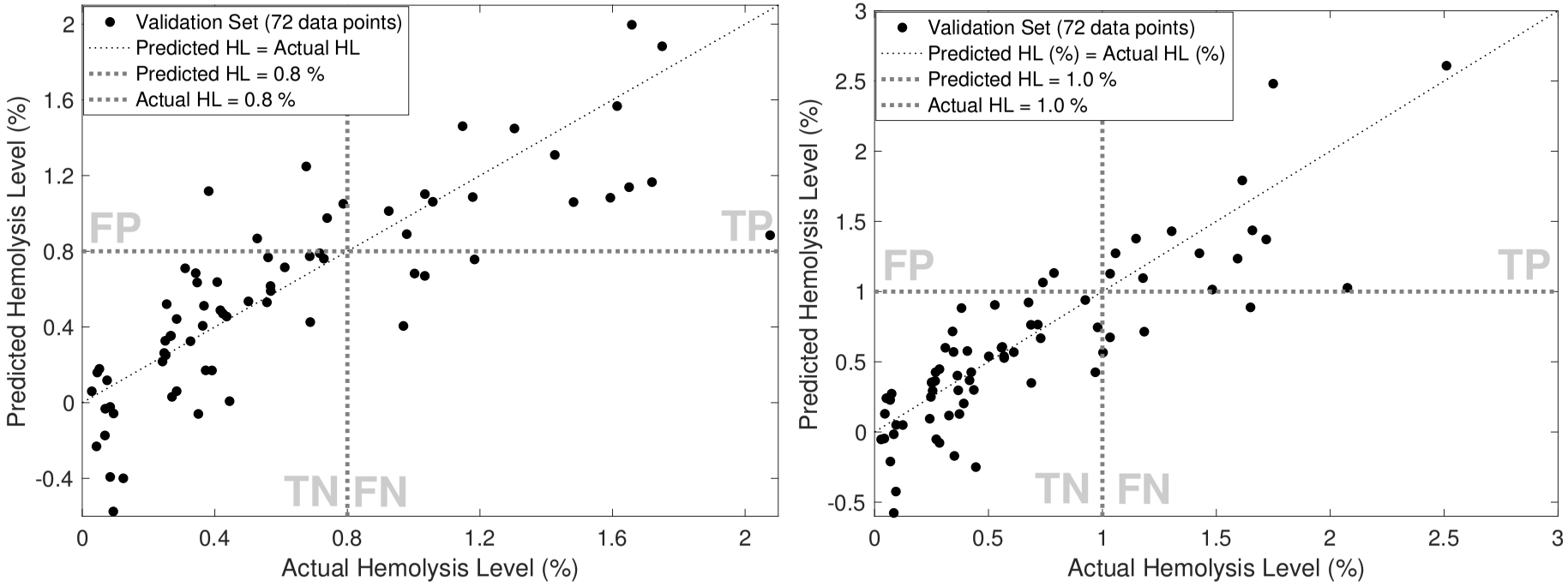

Figure 4.5 Quality assessment of ES units in validation set with the models (a) using reflectance at 518 nm, when 0.8% was used as the threshold hemolysis level and (b) using reflectance at 544 nm, when 1.0% was the threshold. Plots are sketched in form of confusion matrix. Accuracy, sensitivity and specificity of the models can be calculated from the numbers of TP (True positive), TN (True negative), FP (False positive) and FN (False negative) corresponding rectangular quadrants of the graphs.

The model we present for predicting the FHB concentration has an analytical basis. Predictors include diffuse reflectance values and hematological variables of ES that represent their optical properties. All predictors are statistically significant and excluding any of them would influence the accuracy of the prediction, implying that hematological variables alone can not predict the FHB concentration without diffuse reflectance measurements. The quality assessment of blind samples were accurate enough; the error rate of estimating usability of the units was around 10%.

Although the results are promising, due to the following reasons there exist some inaccuracies. In the modeling, the FHB concentration was used as the only source of the increase in $\mu'_{s,EXT}$, but there were numerous particles in the extracellular medium increasing $\mu'_{s,EXT}$ [117]. The optical properties of ES were not physically used; instead, their hematological counterparts were employed. Estimating the optical properties of ES with computational methods such as inverse Monte Carlo would probably provide better results.

Optically measuring the FHB concentration, in the presence of cell interference, has been challenging, and only a few authors have attempted this approach in the past. In one study, the goodness of fit for estimating the hemolysis was evaluated as 0.675 similar to our results [119]. Results of that study could only be improved by fixing the other hematological variables. In a different study, transmission spectra were utilized to predict the FHB concentration, the authors reached R^2=0.9524, but hematological variations in their whole blood samples were not mentioned. As seen throughout this study, there are multiple hematological factors affecting the optical signal collected from blood samples: HCT, Sat-O_2, MCHC. These hematological variables were taken into account in this study and FHB estimation was made on samples with random hematological variables. Fixing these factors or using diluted samples rather than whole blood would obviously make the detection of FHB concentrations much easier. Although aggregation, sedimentation, coagulation and orientation of cells also affect the measured reflectance, they were considered as random error factors.

5. CONCLUSION AND FUTURE DIRECTIONS

For the purpose modeling stored blood quality parameter with non-invasive diffuse reflectance measurements, firstly statistically based mixed linear model was used. However, none of the collected optical parameters accurately modeled hemolysis levels of stored blood. Therefore, an analytical exponential theory was used to express the measured diffuse reflectance from a two-layered turbid samples, like blood in bag, as a function of their optical properties. By this way, the measured diffuse reflectance particularly at 650 nm was modeled most accurately with the hematological variables: MCHC and $SatO_2$. It was observed that the reflectance spectra of ES are mainly characterized by $SatO_2$. Other hematological parameters have limited effects on diffuse reflectance, compared to $SatO_2$. However, the quality related parameters could not be modeled with non-linear exponential model. A semi-empirical equation for diffuse reflectance was finally introduced to model the FHB concentration. The semi-empirical equation was validated with phantom studies and Monte Carlo simulations. With little sacrifice in the accuracy, compared to exponential model, the semi-empirical equation allowed modeling FHB concentration as a linear function of diffuse reflectance and other hematological parameters. Estimations of the quality of blood with the model was accurate at around 90%.

The final proposed model to assess blood quality with diffuse reflectance measurements still requires many hematological parameters as inputs. Other techniques that non-invasively evaluate the hematological variables of blood should be integrated with DRS. In a recent study, the hemoglobin concentration in stored blood was measured non-invasively with the use of transmission and fluorescence spectroscopy [120]. Diffuse reflectance measurements by multiple detectors located at various distances from the source gave accurate HCT levels [121]. The cell counts and volumes could be measured with electrical impedance measurements with pre-located sterile electrodes in bags [122].

The proposed model could also be utilized in other medical fields. Hemolysis is important parameter in clinical analysis; the FHB content of blood samples is the largest source of errors in clinical laboratories. Rather than the time-consuming centrifuging and laboratory tests, with the proposed model the diffuse reflectance measurements can be integrated into hematology analyzers.

These works cover an important step through the next generation in transfusion medicine. In the future, physicians and doctors would know more about the stored units prior to transfusion. For critically ill patients, units with better quality may be administered to reduce transfusion associated negative outcomes.

APPENDIX A. OPTICAL BLOOD PHANTOMS FOR THE ANALYSIS OF REFLECTANCE MEASUREMENTS

A.1 Optical Phantoms to Mimic Human Blood

Optical phantoms contain absorbers, scatterers and a host medium. Ideal absorbers should have low or negligible scattering coefficient and ideal scatterers should not absorb much of the light. The host medium should be optically transparent in the spectral region of interest. In addition, the refractive index of the host medium has to be closer to that of the actual biological sample or tissue [123], namely the blood.

Molecular dyes [124, 125], microscopy stains [126, 127], inorganic salts [128], pen ink [129] and various kinds of pigments [130, 131] are used commonly for creating light-absorbing media. Main consideration in absorber selection is that its absorbance should be linearly proportional to its concentration [132]. For the applications of steady-state DRS, the absorbers of the phantoms should not emit fluorescent or phosphorescent light. Dyes have high water solubility in molecular level, and purely absorb light compared to ink [133]. Ink are composed of carbon particles in size ranges of 100 nm to 1.0 μm, and some of the light is scattered by these particles [129, 134]. The disadvantages of the dyes are their chemical and optical instability [135]. They may interact with the other components in the phantom or lose molecular shapes, which cause shifts in their absorption spectra. Light exposure duration also affects the molar absorption of dyes [136]. However, Indian ink prevails in the aspect of chemical and optical stability [135]. An Indian ink (Pelikan) having two absorption bands below 600 nm and very low absorption beyond 700 nm was used for representing hemoglobin in blood. Absorption spectra of the ink in various concentrations are seen in Figure A.1. The scattering coefficient of ink is assumed to be zero.

Metal oxide particles such as titanium dioxide [137, 138] and aluminum oxide powders [139, 140], fat emulsions [141] and polystyrene latex microspheres [142, 143,

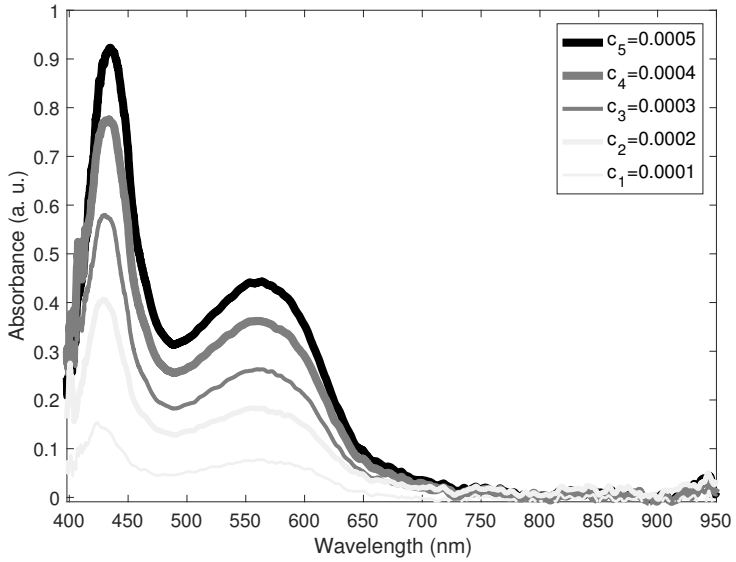

Figure A.1 Absorbance of black Indian ink in visible and NIR spectrum.

144] are generally preferred as scatterers in the phantoms. The metal oxide particles have high sedimentation rate due to their weights and polystyrene particles are very expensive [140]. Fat emulsions are stable for long time [145] and useful for the phantoms in large volumes. Hydrophobic oil forms spherical droplets with diameters ranging from 50 nm to 500 nm causing light scattering in the emulsion [146]. There are numbers of brands for fat emulsions, which are used for feeding patients intravenously: Intralipid® [147, 148], Liposyn® [149], Lipovenoes® [150]. Intralipid® is the widely studied one, and made up of soybean oil, egg yolk phospholipids, glycerin and water [151]. Their batch to batch variances are proved to be low [145]. Their optical properties are theoretically available in the literature, and highly reproducible [151, 152], especially in the concentration range between 2% and 8% where the scattering coefficient of Intralipid®-20% emulsions linearly increases, because in these concentrations the distance between the fat spheres is longer enough than their sizes [146, 153]. This type of light scattering is called "independent scattering" that means the radiance distribution inside the medium is independent of each other [154]. However, when the concentration is higher than 8%, for Intralipid®-20%, the scattering events are dependent to each other and the linear dependency of concentration on the scattering coefficient becomes no longer valid [146, 147, 153]. For low concentrations (c<8%), the

bulk reduced scattering coefficient of Intralipid®-20% in cm^{-1} is given as:

$$\mu_s'(\lambda)/c = -76.7 + 1.71 \times 10^5 \times \lambda^{-0.957} \quad \text{(A.1)}$$

where λ is wavelength in nm [152]. This equation was formulated for 500 nm to 2500 nm, but its validity at much smaller wavelengths has also been shown [151, 155]. The absorption coefficient of Intralipid® is generally neglected [156, 157]; the maximum value is 0.03 cm^{-1} for pure emulsion from the batch. In the NIR region it equals to water absorption [151]. To sum up, the reduced scattering coefficients of the phantoms were determined by the concentration of Intralipid® and the absorption coefficients were determined by the concentration of ink.

A.2 Repeatibility Analysis of Diffuse Reflectance Measurements

Since the diffuse reflectance measurements were performed relative to the diffuse reflectance standard, reliability of the diffuse reflectance standard was examined first. Second, temporal stability of the power of the light source was examined, due to the fact that the diffuse reflectance measurements of multiple ES took several hours. Finally, phantoms having wide optical properties were measured repeatedly under controlled conditions and SD of diffuse reflectance measurements were analyzed.

A.2.1 Reliability of white reflectance standard

The diffuse reflectance standard was placed under the probe holder and the reflected light intensity was recorded across all wavelengths. The recordings were repeated at least ten times, after randomly re-positioning the standard and placing probe holder on it. The coefficient of variation (CV) of multiple measurements were calculated. CV were between 1.3% and 1.8% for the entire spectrum and thier average for all wavelengths was 1.43% (Figure A.2).

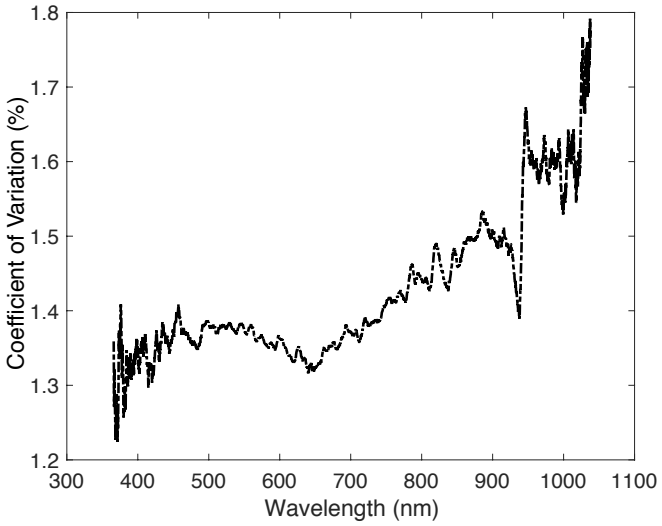

Figure A.2 The repeatibility of the system in measuring the diffuse reflectance standard.

A.2.2 Temporal stability of the light source

The diffuse reflectance standard is actually used to record the spectral power distribution of the light source at the time of the measurement, as reference. However, the spectral power distribution of the light source may change over time due to the temperature increase in the filament or the fluctuations in the line voltage. These may result in shifts in the measured diffuse reflectance.

The temporal stability of the light source was analyzed by recording the reflectance of the diffuse reflectance standard for 2 hours, in 15 minutes intervals. During these recordings, the probe, the probe holder and the reflectance standard positions were not changed. The diffuse reflectance of the standard was recorded as 100% at time = 0, and the spectrum slightly shifted as seen in Figure A.3. The CV was calculated below 0.2% for wavelengths between 400 and 900 nm.

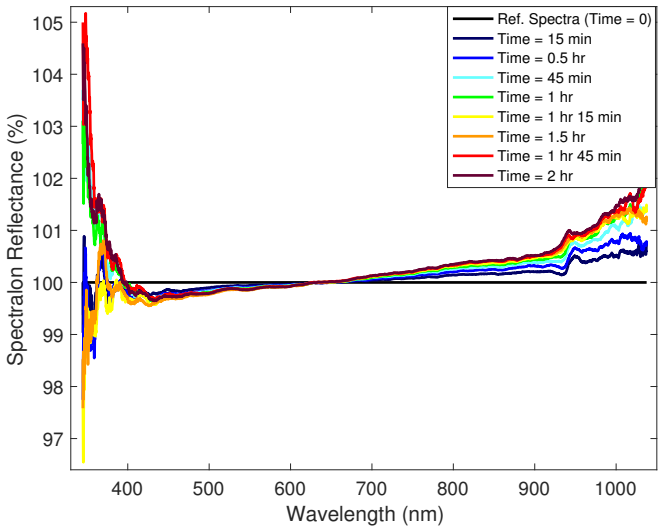

Figure A.3 The shift of the reference spectrum during 2 hours of measurement.

A.2.3 Repeatability of reflectance measurements of phantoms

A total number of 105 phantoms (15 levels of absorption coefficients x 7 levels of reduced scattering coefficients) were used in the repeatibility analysis (Figure A.4). Reflectance measurements were repeated at least ten times and before each recording, the phantoms were picked up, shaken and placed under the probe holder again. The holder was tightened to the post each time from the same height and the pressure of the holder on the blood bag was kept constant by this way.

CV in the reflectance measurements are given in the colored map of the bulk absorption and bulk reduced scattering coefficients of phantoms, between 360 and 1037 nm (Figure A.5). The variances in reflectance measurements seemed random across different optical properties, especially for low absorption levels (μ_a<100 cm^{-1}). In this range, the average CV were below 8% (Figure A.5(a)). For μ_a<70 cm^{-1}, the CV were below 5%. It has become around 2-3% for phantoms with fewer absorption levels. Although, low repeatibility was observed in measuring phantoms having high absorption and reduced scattering coefficients (Figure A.5(b)), the grand average of the coefficient variations for μ_a>100 cm^{-1} was lower than 10%. Indeed, the maximum SD of reflectance was 0.007 (a.u.) (Figure A.5-c and A.5-d), the reason of seeing larger CV (around 30%) was that in high absorption coefficients, reflectance decreased to very low

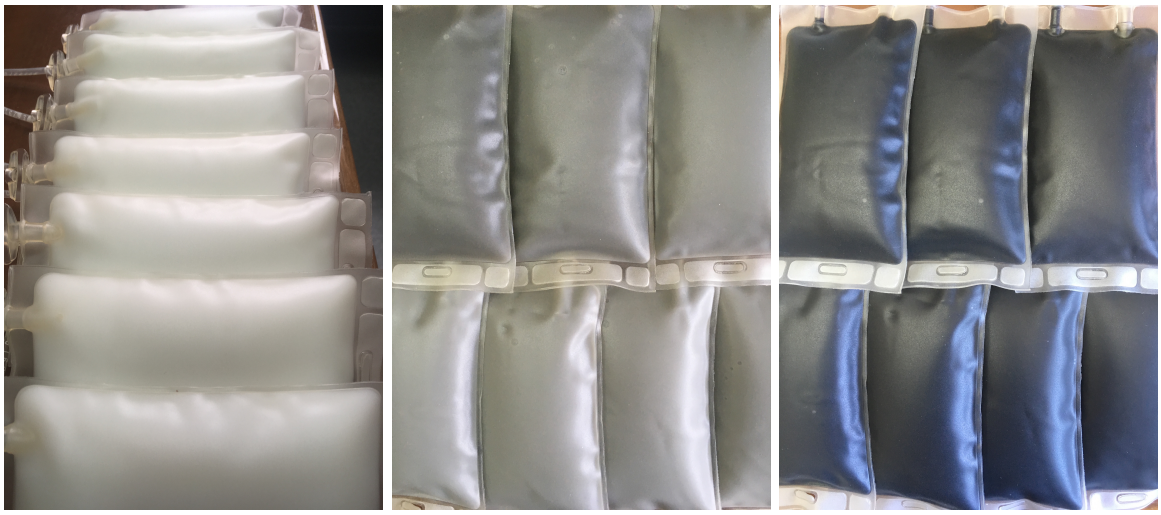

(a) (b) (c)

Figure A.4 .

Illustration of some of the phantoms having; (a) zero, (b) low and (c) high absorption coefficients. In each figure, the scatterer concentrations increase toward right-bottom side

levels. Due to low spectral power of the halogen light source below 400 and above 900 nm wavelengths, the repeatibility of reflectance measurements also decreased beyond these spectral regions. Narrowing the range of repeatibility analysis between 400 and 900 nm gave better results. The maximum CV decreased to 11% and the maximum SD of reflectance decreased to 0.003 (a.u.). With the exception of few occasional measurements, the average CV was below 5% and for very low absorption levels it was even lower than 1% (Figure A.6).

The variances in the reflectance spectra during repeated measurement were not caused only by instrumental errors, but also by random orientation of particles in the phantom, air bubbles in the detection area and the changes in the optical path length contributed by the blood bag due to its elasticity and roughness of the inner surface. The fatty particles in the phantoms were dynamic: the particle density and average volume size inside the optical path may be rippled during each reflectance measurements. Air bubbles might have been in the detection area. The distance and angle between the probe tip and the blood bag might have been different with each

placement. Due to forces exerted to the bag for its mobilization, plastic bags may be squeezed and the thickness may be altered. Moreover, blood bags have also rugged walls that are deliberately created for minimizing the hemolysis. These structures provide highly deformable red cells to escape from outer stresses. The dimensions of these structures are of the same order with the collection fiber diameter (Fig A.7). As a consequence, the displacement of the measuring point on the bag would affect the reflectance signal.

A.2.4 Effect of the contact pressure

The effect of the contact pressure exerted on bags by the probe holder during measurement was analyzed on a set of phantoms having different optical properties.

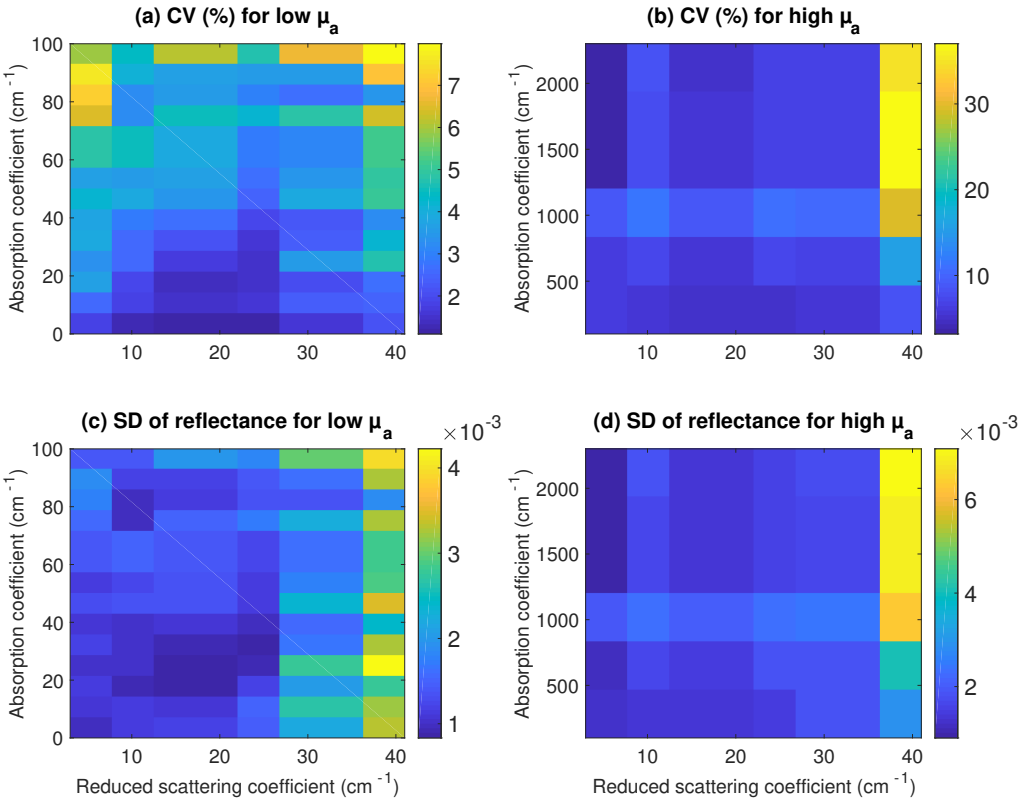

Figure A.5 Repeatibility analysis with measuring phantoms at wavelengths between 360 and 1037 nm.

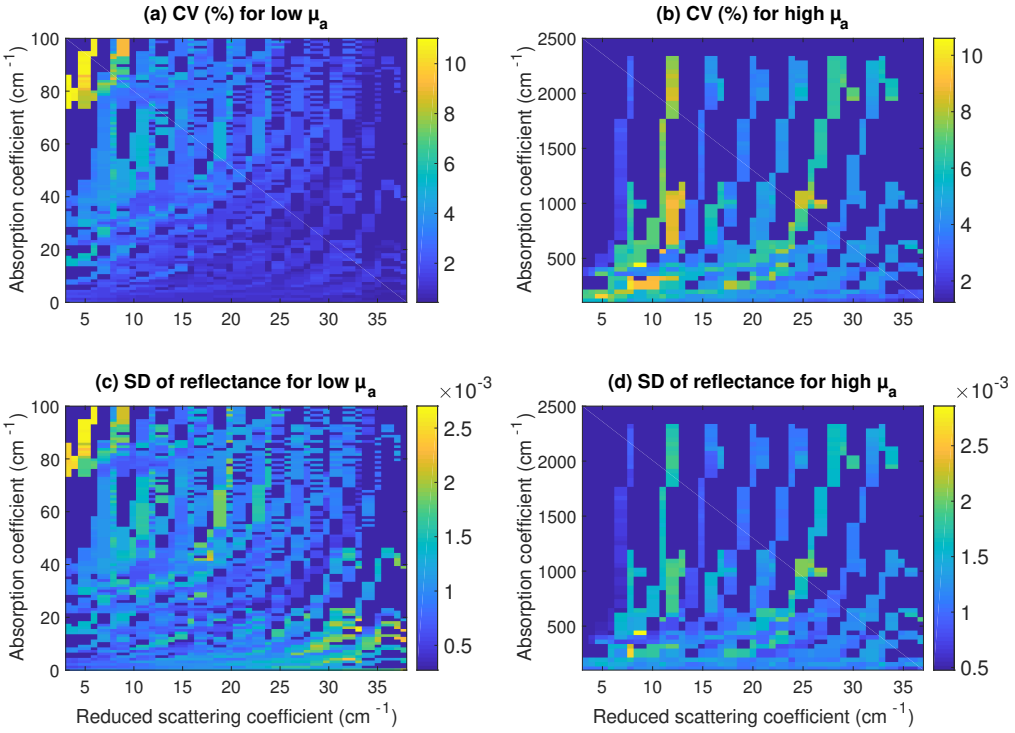

Figure A.6 Repeatibility analysis with measuring phantoms at wavelengths between 400 and 900 nm.

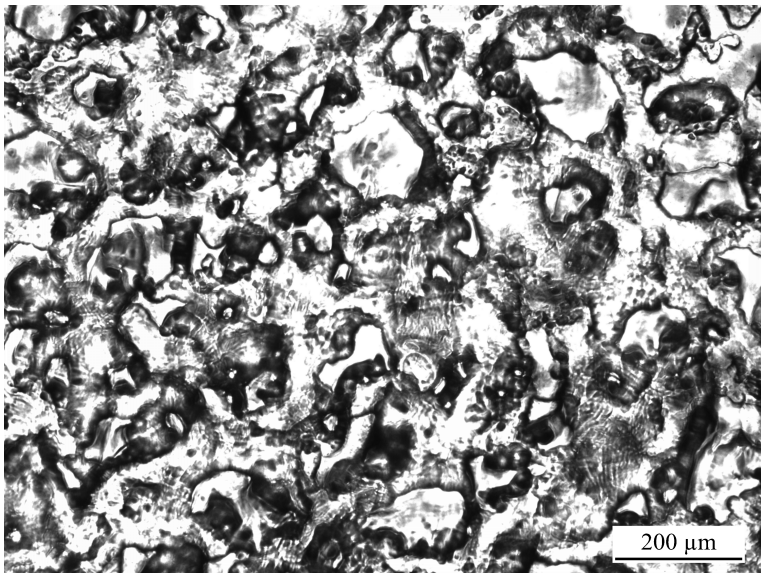

Figure A.7 Image of inner surface of the blood bag (Macopharma, Fr) used in the study, taken with light microscope.

Three pressure levels were assigned as: level-1, level-2 and level-3. The probe holder was pressed against the blood bag by 2, 4 and 6 mm (2 mm being the minimum contact

pressure of the system) and fixed.

The effect of the contact pressure was investigated on a phantom that mimics the optical properties of ES, which has high absorption below 600 nm and low absorption and high scattering level above 600 nm (Figure A.8). The phantom was measured ten times for each pressure level. For each wavelengths between 400 and 900 nm, the contact pressure significantly increased the reflectance spectra ($p<0.01$). The SD of diffuse reflectance was around 0.003 (a.u.) for wavelengths between 400 and 650 nm, but raised to 0.014 (a.u.) in the infrared region and the corresponding CV were 11% and 5% respectively.

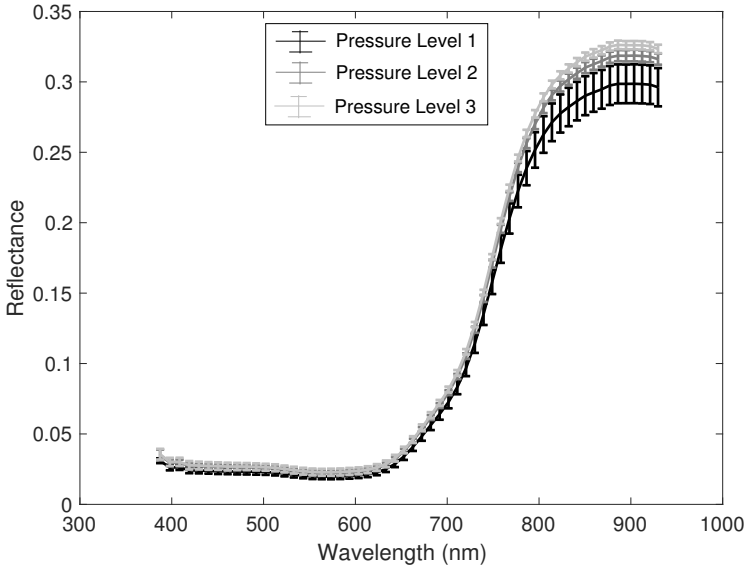

Figure A.8 The effect of the contact pressure on the diffuse reflectance spectrum of the phantom mimicking ES.

A.2.5 Effect of the temperature

To investigate the influence of temperature on the reflectance measurements, a refrigerated phantom was placed under the probe holder and its reflectance was measured while the temperature has risen from $+4\ ^0$C to room temperature ($23\ ^0$C). For comparison, the reflectance of the same phantom was recorded during the measurement period at room temperature.

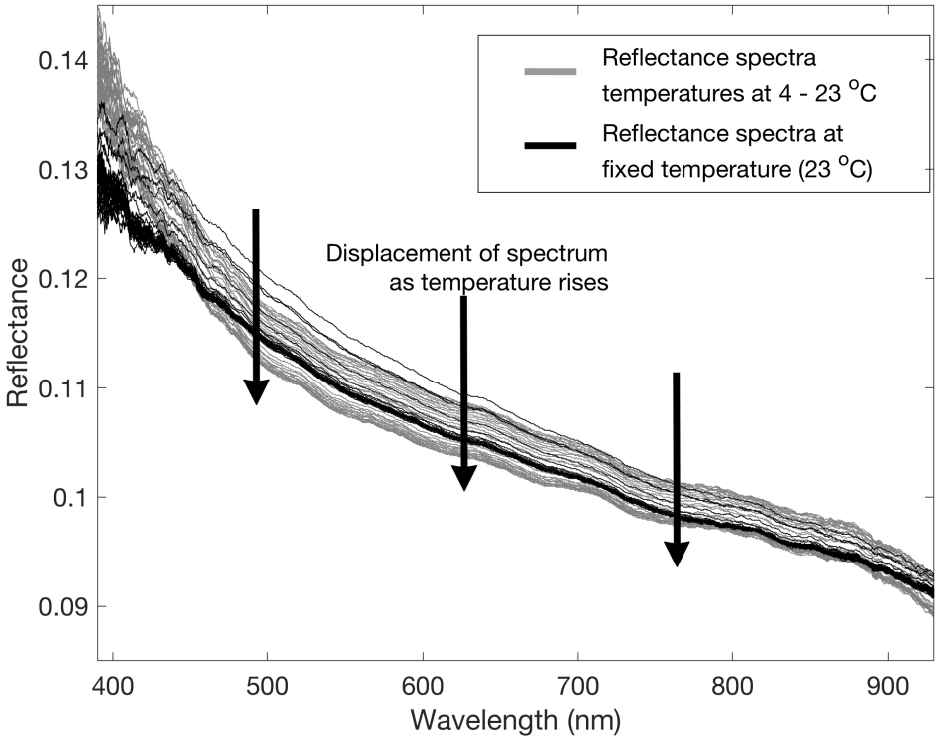

Figure A.9 Change of reflectance spectra with the rise in temperature.

Temperature changes varied the reflectance with maximum SD of 0.003 (a.u.) over the entire spectrum, The SD of diffuse reflectance was 0.002 (a.u.) when the temperature was kept constant at room temperature (23 ^{0}C). The variances in first few measurements were mainly caused by the settlement of the particles in the bag (Figure A.9).

A.3 Effect of the Incident Angle

Throughout the study, 45^0 was used for the angle of incidence with the normal of the bag surface, rather than 0^0. These two measurement configurations were compared. A phantom like ES unit was used in the comparison. The phantom was measured at both incident angles, multiple times, and the repeatibility of the phantoms were considered for comparison.

Normal incident angle caused additional variations in the reflectance measure-

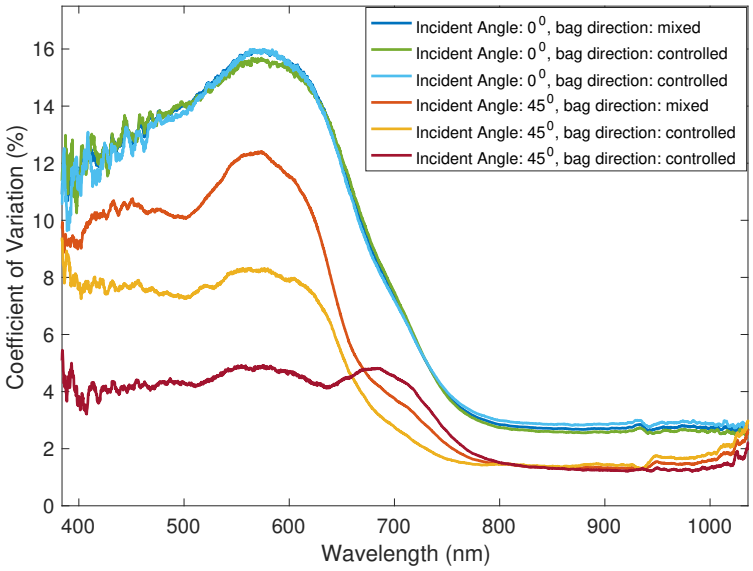

Figure A.10 The effect of the incident angle on the repeatibility of the diffuse reflectance measurements.

ments. The main reason of these variations was the specular reflection. For normal incident angle, the measured reflectance would become the sum of the diffuse and specular reflections. However, the specular reflection is mirror-like reflection and do not rely on optical properties of ES. The specular reflection can be avoided by changing the angle of incidence to 45^0. Eliminating specular reflection decreased the standard error as seen in Figure A.10. The standard error further decreased ($<5\%$) by controlling the orientation of the bag while placing it under the probe holder. It was observed that controlling orientation was only effective with the angle of incidence of 45^0. When the incident light is directed with an oblique angle, light path in the blood bag is longer than its normal thickness. Obviously, the path is not symmetrical in all directions. Variations in diffuse reflectance spectra while the bag was placed toward different directions (left or right) are seen in Figure A.11. The variations were most probably related to the blood bag and they were visible below 600 nm where the absorption of the phantoms were higher.

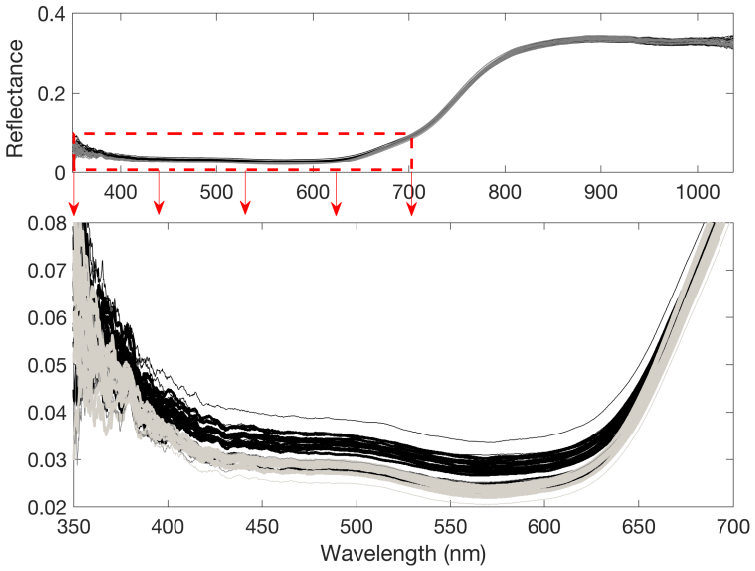

Figure A.11 Variations in the reflectance measurements, at 45^0 incident angle, when placing the bag toward two different directions.

A.4 Effect of Refractive Index Mismatch

The blood bag and ES have different refractive indices, causing multiple reflections at the bag and blood interface. The effect of this refractive index mismatch was investigated by measuring reflectance of blood bag filled with non-absorbing and non-scattering medium such as distilled water or pressured air. Glass was also tried as the second layer, after cutting a sheet of bag and sticking it on a 1-cm thick glass.

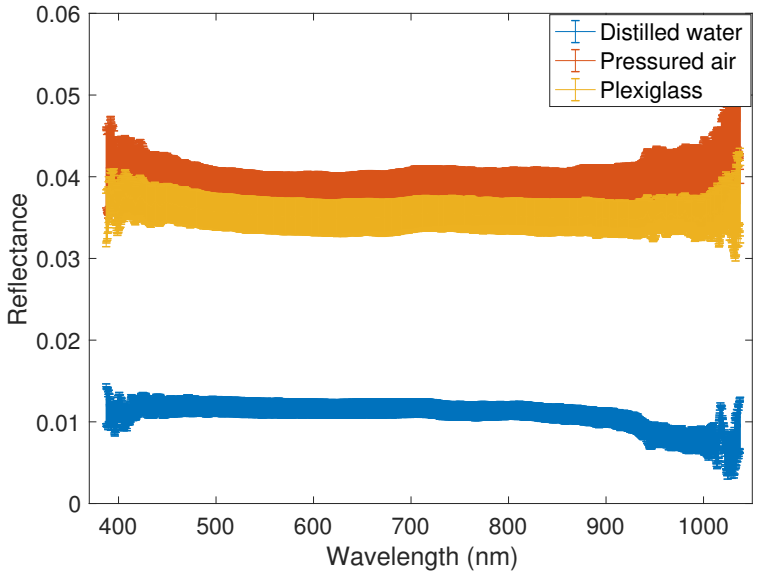

Figure A.12 Reflectance measurements under different refractive index mismatch conditions.

As it was expected, SD in repeated measurements of transparent materials were very high, but the results still exhibited the effect of the refractive index on the reflectance spectra. The variations in the reflectance values were caused by the refractive index mismatch between the bag and the layer below it.

A.5 Detection and Quantification Limits for the Lowest Concentration of Scattering Particles

The semi-empirical equation for the reflectance theory suggests that the reduced scattering coefficient of the sample is linearly proportional to the measured reflectance. For such linear systems, the detection and quantification limits are the important characteristics. The detection limit for the lowest concentration of scattering particles was calculated from the following equation [158]:

$$\begin{aligned} DL &= 3.3 \times \frac{\sigma}{s} \\ QL &= 10 \times \frac{\sigma}{s} \end{aligned} \tag{A.2}$$

σ in the equation can be (1) the SD of reflectance spectra of blank (distilled water), (2) the standard error of estimate for calibration intercept or (3) the residual SD for the calibration line. s in the equation corresponds to the slope of the calibration line.

The limit of the reflectance measurement in quantification (the lowest concentration of Intralipid®-20%) was found as 0.0065 mL/mL, by using $1/k_2$ from Eq. 4.2, as a replace of s in Eq. A.2. The obtained concentration corresponds to reduced scattering coefficients between 1 - 3.5 cm^{-1}, according to Eq. A.1.

APPENDIX B. LIST OF PUBLICATIONS PRODUCED FROM THE DISSERTATION

1. Osman Melih Can, Yekta Ülgen, Ata Akın "Monitoring of diffuse reflectance spectra of erythrocyte suspensions during storage,"2017 21st National Biomedical Engineering Meeting (BIYOMUT), (24 Nov.-26 Dec.2017), DOI: 10.1109/BIYOMUT.2017.8479000

2. Osman Melih Can, Yekta Ülgen, "Estimation of free hemoglobin concentrations in blood bags by diffuse reflectance spectroscopy,"J. Biomed. Opt. 23(12), 127001 (2018), doi: 10.1117/1.JBO.23.12.127001.

3. Osman Melih Can, Yekta Ülgen "Modeling diffuse reflectance spectra of donated blood with their hematological parameters,"Proc. SPIE 11074, Diffuse Optical Spectroscopy and Imaging VII, 110741T (11 July 2019); doi:10.1117/12.2526848

REFERENCES

1. Blundell, J., *Researches Physiological and Pathological; Instituted Principally with a View to the Improvement of Medical and Surgical Practice*, London: S. & R. Bentley, 1824.

2. Pavenski, K., E. Saidenberg, M. Lavoie, M. Tokessy, and D. R. Branch, "Red blood cell storage lesions and related transfusion issues: A Canadian Blood Services Research and Development Symposium," *Transfusion Medicine Reviews*, Vol. 26, no. 1, pp. 68–84, 2012.

3. Zaaijer, H. L., "Prevention of transfusion-transmitted infections: Dilemmas," *Frontiers in Medicine*, Vol. 4, no. Dec., pp. 1–3, 2017.

4. Yoshida, T., M. Prudent, and A. D'Alessandro, "Red blood cell storage lesion: Causes and potential clinical consequences," *Blood Transfusion*, Vol. 17, no. 1, pp. 27–52, 2019.

5. Hess, J. R., "Red cell changes during storage," *Transfusion and Apheresis Science*, Vol. 43, no. 1, pp. 51–59, 2010.

6. Triulzi, D. J., and M. H. Yazer, "Clinical studies of the effect of blood storage on patient outcomes," *Transfusion and Apheresis Science*, Vol. 43, no. 1, pp. 95–106, 2010.

7. Keller, M. E., R. Jean, W. W. LaMorte, F. Millham, and E. Hirsch, "Effects of age of transfused blood on length of stay in trauma patients: A preliminary report," *Journal of Trauma*, Vol. 53, no. 5, pp. 1023–5, 2002.

8. Marik, P. E., and W. J. Sibbald, "Effect of stored-blood transfusion on oxygen delivery in patients with sepsis," *JAMA: The Journal of the American Medical Association*, Vol. 269, no. 23, pp. 3024–9, 1993.

9. Purdy, F. R., M. G. Tweeddale, and P. M. Merrick, "Association of mortality with age of blood transfused in septic ICU patients," *Canadian Journal of Anaesthesia*, Vol. 44, no. 12, pp. 1256–61, 1997.

10. Zallen, G., P. J. Offner, E. E. Moore, J. Blackwell, D. J. Ciesla, J. Gabriel, C. Denny, and C. C. Silliman, "Age of transfused blood is an independent risk factor for postinjury multiple organ failure," *American Journal of Surgery*, Vol. 178, no. 6, pp. 570–2, 1999.

11. Murrell, Z., J. S. Haukoos, B. Putnam, and S. R. Klein, "The effect of older blood on mortality, need for ICU care, and the length of ICU stay after major trauma," *American Surgeon*, Vol. 71, no. 9, pp. 781–5, 2005.

12. Koch, C. G., L. Li, D. I. Sessler, P. Figueroa, G. A. Hoeltge, T. Mihaljevic, and E. H. Blackstone, "Duration of red-cell storage and complications after cardiac surgery," *New England Journal of Medicine*, Vol. 358, no. 12, pp. 1229–1239, 2008.

13. Kiraly, L. N., S. Underwood, J. A. Differding, and M. A. Schreiber, "Transfusion of aged packed red blood cells results in decreased tissue oxygenation in critically injured trauma patients," *Journal of Trauma - Injury, Infection and Critical Care*, Vol. 67, no. 1, pp. 29–32, 2009.

14. Spinella, P. C., C. L. Carroll, I. Staff, R. Gross, J. Mc Quay, L. Keibel, C. E. Wade, and J. B. Holcomb, "Duration of red blood cell storage is associated with increased incidence of deep vein thrombosis and in hospital mortality in patients with traumatic injuries," *Critical Care*, Vol. 13, no. 5, p. R151, 2009.

15. Robinson, S. D., C. Janssen, E. B. Fretz, B. Berry, A. J. Chase, A. D. Siega, R. G. Carere, A. Fung, G. Simkus, W. P. Klinke, and J. D. Hilton, "Red blood cell storage duration and mortality in patients undergoing percutaneous coronary intervention," *American Heart Journal*, Vol. 159, no. 5, pp. 876–881, 2010.

16. Pettilä, V., A. J. Westbrook, A. D. Nichol, M. J. Bailey, E. M. Wood, G. Syres, L. E. Phillips, A. Street, C. French, L. Murray, N. Orford, J. D. Santamaria, R. Bellomo, and D. J. Cooper, "Age of red blood cells and mortality in the critically ill," *Critical Care*, Vol. 15, no. 2, p. R116, 2011.

17. Weinberg, J. A., G. McGwin, M. B. Marques, S. A. Cherry, D. A. Reiff, J. D. Kerby, and L. W. Rue, "Transfusions in the less severely injured: Does age of transfused blood affect outcomes?," *Journal of Trauma - Injury, Infection and Critical Care*, Vol. 65, no. 4, pp. 794–798, 2008.

18. Weinberg, J. A., G. McGwin, R. L. Griffin, V. Q. Huynh, S. A. Cherry, M. B. Marques, D. A. Reiff, J. D. Kerby, and L. W. Rue, "Age of transfused blood: An independent predictor of mortality despite universal leukoreduction," *Journal of Trauma - Injury, Infection and Critical Care*, Vol. 65, no. 2, pp. 279–282, 2008.

19. Weinberg, J. A., G. McGwin, M. J. Vandromme, M. B. Marques, S. M. Melton, D. A. Reiff, J. D. Kerby, and L. W. Rue, "Duration of red cell storage influences mortality after trauma," *Journal of Trauma - Injury, Infection and Critical Care*, Vol. 69, no. 6, pp. 1427–31, 2010.

20. Eikelboom, J. W., R. J. Cook, Y. Liu, and N. M. Heddle, "Duration of red cell storage before transfusion and in-hospital mortality," *American Heart Journal*, Vol. 159, no. 5, pp. 737–743.e1, 2010.

21. Gauvin, F., P. C. Spinella, J. Lacroix, G. Choker, T. Ducruet, O. Karam, P. C. Hébert, J. S. Hutchison, H. A. Hume, and M. Tucci, "Association between length of storage of transfused red blood cells and multiple organ dysfunction syndrome in pediatric intensive care patients," *Transfusion*, Vol. 50, no. 9, pp. 1902–1913, 2010.

22. Sanders, J., S. Patel, J. Cooper, J. Berryman, D. Farrar, M. Mythen, and H. E. Montgomery, "Red blood cell storage is associated with length of stay and renal complications after cardiac surgery," *Transfusion*, Vol. 51, no. 11, pp. 2286–2294, 2011.

23. Katsios, C., L. Griffith, P. Spinella, J. Lacroix, M. Crowther, P. Hebert, M. Meade, W. Geerts, C. Rabbat, and D. Cook, "Red blood cell transfusion and increased length of storage are not associated with deep vein thrombosis in medical and surgical critically ill patients: a prospective observational cohort study," *Critical Care*, Vol. 15, no. 6, p. R263, 2011.

24. McKenny, M., T. Ryan, H. Tate, B. Graham, V. K. Young, and N. Dowd, "Age of transfused blood is not associated with increased postoperative adverse outcome after cardiac surgery," *British Journal of Anaesthesia*, Vol. 106, no. 5, pp. 643–9, 2011.

25. Van Straten, A. H., M. A. Soliman Hamad, A. A. Van Zundert, E. J. Martens, J. F. Ter Woorst, A. M. De Wolf, and V. Scharnhorst, "Effect of duration of red blood cell storage on early and late mortality after coronary artery bypass grafting," *Journal of Thoracic and Cardiovascular Surgery*, Vol. 141, no. 1, pp. 231–7, 2011.

26. Aubron, C., A. Nichol, D. J. Cooper, and R. Bellomo, "Age of red blood cells and transfusion in critically ill patients," *Annals of Intensive Care*, Vol. 3, no. 1, p. 2, 2013.

27. Lelubre, C., and J.-L. Vincent, "Relationship between red cell storage duration and outcomes in adults receiving red cell transfusions: a systematic review," *Critical Care*, Vol. 17, no. 2, p. R66, 2013.

28. Chai-Adisaksopha, C., P. E. Alexander, G. Guyatt, M. A. Crowther, N. M. Heddle, P. J. Devereaux, M. Ellis, D. Roxby, D. I. Sessler, and J. W. Eikelboom, "Mortality outcomes in patients transfused with fresher versus older red blood cells: a meta-analysis," *Vox Sanguinis*, Vol. 112, no. 3, pp. 268–278, 2017.

29. Lacroix, J., P. C. Hébert, D. A. Fergusson, and et. al., "Age of transfused blood in critically ill adults," *New England Journal of Medicine*, Vol. 372, no. 15, pp. 1410–1418, 2015. PMID: 25853745.

30. Steiner, M. E., P. M. Ness, S. F. Assmann, and et. al., "Effects of red-cell storage duration on patients undergoing cardiac surgery," *New England Journal of Medicine*, Vol. 372, no. 15, pp. 1419–1429, 2015. PMID: 25853746.

31. Cooper, D. J., Z. K. McQuilten, A. Nichol, and et. al., "Age of red cells for transfusion and outcomes in critically ill adults," *New England Journal of Medicine*, Vol. 377, no. 19, pp. 1858–1867, 2017. PMID: 28952891.

32. Berezina, T. L., S. B. Zaets, C. Morgan, C. R. Spillert, M. Kamiyama, Z. Spolarics, E. A. Deitch, and G. W. Machiedo, "Influence of storage on red blood cell rheological properties," *Journal of Surgical Research*, Vol. 102, no. 1, pp. 6–12, 2002.

33. Beutler, E., W. Kuhl, and C. West, "The osmotic fragility of erythrocytes after prolonged liquid storage and after reinfusion," *Blood*, Vol. 59, no. 6, pp. 1141–1147, 1982.

34. Barshtein, G., D. Arbell, and S. Yedgar, "Hemodynamic functionality of transfused red blood cells in the microcirculation of blood recipients," *Frontiers in Physiology*, Vol. 9, no. Jan., pp. 1–6, 2018.

35. Chin-Yee, I., N. Arya, and M. S. D'Almeida, "The red cell storage lesion and its implication for transfusion," *Transfusion Science*, Vol. 18, no. 3, pp. 447–458, 1997.

36. Barshtein, G., N. Manny, and S. Yedgar, "Circulatory risk in the transfusion of red blood cells with impaired flow properties induced by storage," *Transfusion Medicine Reviews*, Vol. 25, no. 1, pp. 24–35, 2011.

37. Donadee, C., N. J. H. Raat, T. Kanias, and et. al., "Nitric oxide scavenging by red blood cell microparticles and cell-free hemoglobin as a mechanism for the red cell storage lesion," *Circulation*, Vol. 124, no. 4, pp. 465–476, 2011.

38. Neal, M. D., J. S. Raval, D. J. Triulzi, and R. L. Simmons, "Innate immune activation after transfusion of stored red blood cells," *Transfusion Medicine Reviews*, Vol. 27, no. 2, pp. 113–118, 2013.

39. Rapido, F., "The potential adverse effects of haemolysis," *Blood Transfusion*, Vol. 15, no. 3, pp. 218–221, 2017.

40. Hod, E. A., N. Zhang, S. A. Sokol, B. S. Wojczyk, R. O. Francis, D. Ansaldi, K. P. Francis, P. Della-Latta, S. Whittier, S. Sheth, J. E. Hendrickson, J. C. Zimring, G. M. Brittenham, and S. L. Spitalnik, "Transfusion of red blood cells after prolonged storage produces harmful effects that are mediated by iron and inflammation," *Blood*, Vol. 115, no. 21, pp. 4284–92, 2010.

41. Baron, D. M., B. Yu, C. Lei, A. Bagchi, A. Beloiartsev, C. P. Stowell, A. U. Steinbicker, R. Malhotra, K. D. Bloch, and W. M. Zapol, "Pulmonary hypertension in lambs transfused with stored blood is prevented by breathing nitric oxide," *Anesthesiology*, Vol. 116, no. 3, pp. 637–47, 2012.

42. Yu, B., C. Lei, D. M. Baron, A. U. Steinbicker, K. D. Bloch, and W. M. Zapol, "Diabetes augments and inhaled nitric oxide prevents the adverse hemodynamic effects of transfusing syngeneic stored blood in mice," *Transfusion*, Vol. 52, no. 7, pp. 1410–22, 2012.

43. Leal-Noval, S. R., M. Muñoz-Gómez, V. Arellano-Orden, A. Marín-Caballos, R. Amaya-Villar, A. Marín, A. Puppo-Moreno, C. Ferrándiz-Millón, J. M. Flores-Cordero, and F. Murillo-Cabezas, "Impact of age of transfused blood on cerebral oxygenation in male patients with severe traumatic brain injury," *Critical Care Medicine*, Vol. 36, no. 4, pp. 1290–6, 2008.

44. Ayhan, B., K. Yuruk, S. Koene, A. Sahin, C. Ince, and U. Aypar, "The effects of non-leukoreduced red blood cell transfusions on microcirculation in mixed surgical patients," *Transfusion and Apheresis Science*, Vol. 49, no. 2, pp. 212–22, 2013.

45. Damiani, E., E. Adrario, M. M. Luchetti, C. Scorcella, A. Carsetti, N. Mininno, S. Pierantozzi, T. Principi, D. Strovegli, R. Bencivenga, A. Gabrielli, R. Romano, P. Pelaia, C. Ince, and A. Donati, "Plasma free hemoglobin and microcirculatory response to fresh or old blood transfusions in sepsis," *PLoS ONE*, Vol. 10, no. 5, p. e0122655, 2015.

46. Council of Europe, *Guide to the Preparation, Use and Quality Assurance of Blood Components*, Strasbourg, France: European Directorate for the Quality of Medicines & HealthCare (EDQM), 19th ed., 2017.

47. Högman, C. F., and H. T. Meryman, "Storage parameters affecting red blood cell survival and function after transfusion," *Transfusion Medicine Reviews*, Vol. 13, no. 4, pp. 275–296, 1999.

48. Hess, J. R., R. L. Sparrow, P. F. Van Der Meer, J. P. Acker, R. A. Cardigan, and D. V. Devine, "Red blood cell hemolysis during blood bank storage: Using national quality management data to answer basic scientific questions," *Transfusion*, Vol. 49, no. 12, pp. 2599–2603, 2009.

49. Canadian Blood Services, *Visual Assessment Guide*, January 2009.

50. Janatpour, K. A., T. G. Paglieroni, V. L. Crocker, D. J. DuBois, and P. V. Holland, "Visual assessment of hemolysis in red blood cell units and segments can be deceptive," *Transfusion*, Vol. 44, no. 7, pp. 984–989, 2004.

51. Kanias, T., and M. T. Gladwin, "Nitric oxide, hemolysis, and the red blood cell storage lesion: Interactions between transfusion, donor, and recipient," *Transfusion*, Vol. 52, no. 7, pp. 1388–1392, 2012.

52. Tzounakas, V. L., H. T. Georgatzakou, A. G. Kriebardis, A. I. Voulgaridou, K. E. Stamoulis, L. E. Foudoulaki-Paparizos, M. H. Antonelou, and I. S. Papassideri, "Donor variation effect on red blood cell storage lesion: A multivariable, yet consistent, story," *Transfusion*, Vol. 56, no. 6, pp. 1274–1286, 2016.

53. Kanias, T., M. C. Lanteri, G. P. Page, and et. al., "Ethnicity, sex, and age are determinants of red blood cell storage and stress hemolysis: Results of the REDS-III RBC-Omics study," *Blood Advances*, Vol. 1, no. 15, pp. 1132–1141, 2017.

54. Dunbar, N. M., N. J. Olson, Z. M. Szczepiorkowski, E. D. Martin, R. M. Tysarcyk, D. J. Triulzi, L. H. Alarcon, and M. H. Yazer, "Blood component transfusion and wastage rates in the setting of massive transfusion in three regional trauma centers," *Transfusion*, Vol. 57, no. 1, pp. 45–52, 2017.

55. Shamshirian, A., A. R. Mohseni, A. A. Pourfathollah, S. Mehdipour, S. Hosseini, A. Ghorbanpour, and S. Azizi, "A review of blood usage and wastage in a tertiary heart center," *Acta Clinica Belgica*, pp. 1–8, 2018.

56. DeSimone, R. A., M. D. Nowak, D. T. Lo, K. M. Crowley, P. Parra, M. M. Cushing, and Y. M. S. Hsu, "Logistical and safety implications of temperature-based acceptance of returned red blood cell units," *Transfusion*, Vol. 58, no. 6, pp. 1500–1505, 2018.

57. Meinke, M. C., M. Friebel, J. Helfmann, and M. Notter, "A novel device for the non-invasive measurement of free hemoglobin in blood bags / Messgerät zur zerstörungsfreien Messung von freiem Hämoglobin in Blutkonserven," *Biomedizinische Technik/Biomedical Engineering*, Vol. 50, no. 1-2, pp. 2–7, 2005.

58. Buckley, K., C. G. Atkins, D. Chen, H. G. Schulze, D. V. Devine, M. W. Blades, and R. F. B. Turner, "Non-invasive spectroscopy of transfusable red blood cells stored inside sealed plastic blood-bags," *Analyst*, Vol. 141, no. 5, pp. 1678–85, 2016.

59. Vardaki, M. Z., C. G. Atkins, H. G. Schulze, D. V. Devine, K. Serrano, M. W. Blades, and R. F. Turner, "Raman spectroscopy of stored red blood cell concentrate within sealed transfusion blood bags," *Analyst*, Vol. 143, no. 24, pp. 6006–6013, 2018.

60. Pinto, R. N., E. Hysi, K. Bagga, J. A. Sebastian, A. Douplik, J. P. Acker, and M. C. Kolios, "Feasibility of photoacoustic imaging for the non-invasive quality management of stored blood bags," *Vox Sanguinis*, Vol. 114, no. July, pp. 701–710, 2019.

61. Can, O. M., Y. Ülgen, and A. Akın, "Use of the color spaces in determining the level of hemolysis in blood under storage," in *IFMBE Proceedings* (Lackovic, I., and D. Vasic, eds.), (Dubrovnik, Croatia), pp. 290–293, 2015.

62. Sağlık Bakanlığı, "Ulusal Kan ve Kan Bileşenleri Hazırlama, Kullanım, Kalite Güvencesi Rehberi," pp. 1–293, 2016.

63. Han, V., K. Serrano, and D. V. Devine, "A comparative study of common techniques used to measure haemolysis in stored red cell concentrates," *Vox Sanguinis*, Vol. 98, no. 2, pp. 116–123, 2010.

64. Noe, D. A., V. Weedn, and W. R. Bell, "Direct spectrophotometry of serum hemoglobin: an Allen correction compared with a three-wavelength polychromatic analysis," *Clinical Chemistry*, Vol. 30, no. 5, pp. 627–30, 1984.

65. Blackwell, E., C. F. M. de Leon, and G. E. Miller, "Applying mixed regression models to the analysis of repeated-measures data in psychosomatic medicine," *Psychosomatic medicine*, Vol. 68, no. 6, pp. 870–8, 2006.

66. Martelli, F., S. D. Bianco, A. Ismaelli, and G. Zaccanti, *Light Propagation through Biological Tissue and Other Diffusive Media: Theory, Solutions, and Software*, Bellingham, Washington, USA: SPIE PRESS, 2009.

67. Chandrasekhar, S., *Radiative Transfer*, New York: Dover Publications, 1960.

68. Seo, I. S., C. K. Hayakawa, and V. Venugopalan, "Radiative transport in the delta-P1 approximation for semi-infinite turbid media," *Medical Physics*, Vol. 35, no. 2, pp. 681–93, 2008.

69. Wang, L., Jacques, S. L., & Zheng, L., "MCML - Monte Carlo modeling of light transport in multi-layered tissues," *Computer Methods and Programs in Biomedicine*, Vol. 47, no. 2, pp. 131–146, 1995.

70. Sandoval, C., and A. D. Kim, "Deriving kubelka-munk theory from radiative transport," *Journal of the Optical Society of America A*, Vol. 31, pp. 628–636, Mar. 2014.

71. Splinter, R., and B. A. Hooper, *An Introduction to Biomedical Optics*, Baco Raton, FL: Taylor & Francis, 2007.

72. Wilson, R. H., and M. A. Mycek, "Models of light propagation in human tissue applied to cancer diagnostics," *Technology in Cancer Research and Treatment*, Vol. 10, no. 2, pp. 121–134, 2011.

73. Naglič, P., L. Vidovič, M. Milanič, L. L. Randeberg, and B. Majaron, "Applicability of diffusion approximation in analysis of diffuse reflectance spectra from healthy human skin," in *Biophotonics—Riga 2013* (Spigulis, J., and I. Kuzmina, eds.), Vol. 9032, pp. 137 – 148, International Society for Optics and Photonics, SPIE, 2013.

74. Wang, L., and H. Wu, *Biomedical Optics: Principles and Imaging*, New Jersey: John Wiley & Sons, 2007.

75. Bosschaart, N., G. J. Edelman, M. C. G. Aalders, T. G. Van Leeuwen, and D. J. Faber, "A literature review and novel theoretical approach on the optical properties of whole blood," *Lasers in Medical Science*, Vol. 29, no. 2, pp. 453–479, 2014.

76. Farrell, T. J., M. S. Patterson, and B. Wilson, "A diffusion Theory Model of Spatially Resolved, Steady-State Diffuse Reflectance for the Noninvasive Determination of Tissue Optical Properties in Vivo," *Medical Physics*, Vol. 19, no. 4, pp. 879–88, 1992.

77. Wu, J., F. Partovi, M. S. Field, and R. P. Rava, "Diffuse reflectance from turbid media: an analytical model of photon migration," *Applied Optics*, Vol. 32, no. 7, pp. 1115–21, 1993.

78. Perelman, L. T., J. Wu, I. Itzkan, and M. S. Feld, "Photon migration in turbid media using path integrals," *Physical Review Letters*, Vol. 72, no. 9, pp. 1341–1344, 1994.

79. Zonios, G., and A. Dimou, "Modeling diffuse reflectance from semi-infinite turbid media: application to the study of skin optical properties," *Optics Express*, Vol. 14, no. 19, pp. 8661–8674, 2006.

80. Zonios, G. I., *Diffuse Reflectance Spectroscopy of Human Colon Tissue*. PhD thesis, Massaschusetts Institute of Technology, Maryland, US, 1998.

81. Hérault, O., C. Binet, A. Rico, M. Degenne, M. C. Bernard, M. Chassaigne, and L. Sensebe, "Evaluation of performance of white blood cell reduction filters: An original flow cytometric method for detection and quantification of cell-derived membrane fragments," *Cytometry*, Vol. 45, no. 4, pp. 277–84, 2001.

82. Loi, M. M., M. Kelher, M. Dzieciatkowska, K. C. Hansen, A. Banerjee, F. B. West, C. Stanley, M. Briel, and C. C. Silliman, "A comparison of different methods of red blood cell leukoreduction and additive solutions on the accumulation of neutrophil-priming activity during storage," *Transfusion*, Vol. 58, no. 8, pp. 2003–2012, 2018.

83. Keys, A., "The oxygen saturation of the venous blood in normal human subjects," *American Journal of Physiology*, Vol. 124, no. Sep., pp. 13–21, 1938.

84. Meinke, M., G. Müller, J. Helfmann, and M. Friebel, "Optical properties of platelets and blood plasma and their influence on the optical behavior of whole blood in the visible to near infrared wavelength range," *Journal of Biomedical Optics*, Vol. 12, no. 1, 2015.

85. Prahl, S., "Tabulated Molar Extinction Coefficient for Hemoglobin in Water," tech. rep., https://omlc.org/spectra/hemoglobin/summary.html, 1998.

86. Steinke, J. M., and a. P. Shepherd, "Comparison of Mie theory and the light scattering of red blood cells," *Applied Optics*, Vol. 27, no. 19, pp. 4027–4033, 1988.

87. Bohren, C. F., and D. R. Huffman, *Absorption and Scattering of Light by Small Particles*, John Wiley & Sons, 1983.

88. Reynolds, L., C. Johnson, and A. Ishimaru, "Diffuse reflectance from a finite blood medium: applications to the modeling of fiber optic catheters," *Applied Optics*, Vol. 15, no. 9, pp. 2059–2067, 1976.

89. Borovoi, A. G., E. I. Naats, and U. G. Oppel, "Scattering of light by a red blood cell," *Journal of Biomedical Optics*, Vol. 3, no. 3, pp. 364 – 372, 1998.

90. Can, O. M., and Y. Ülgen, "Estimation of free hemoglobin concentrations in blood bags by diffuse reflectance spectroscopy," *Journal of Biomedical Optics*, Vol. 23, no. 12, 2018.

91. Prahl, S. A., M. J. C. van Gemert, and A. J. Welch, "Determining the optical properties of turbid media by using the adding-doubling method," *Applied Optics*, Vol. 32, no. 4, pp. 559–568, 1993.

92. Can, O. M., and Y. Ülgen, "Modeling diffuse reflectance spectra of donated blood with their hematological parameters," in *Clinical and Preclinical Optical Diagnostics II*, no. 11074-62, (Munich, Germany), European Conferences on Biomedical Optics, SPIE-OSA, 25-29 June 2019.

93. Sircan-Kucuksayan, A., M. Uyuklu, and M. Canpolat, "Diffuse reflectance spectroscopy for the measurement of tissue oxygen saturation," *Physiological Measurement*, Vol. 36, no. 12, pp. 2461–2469, 2015.

94. O'Connor, T. M., P. J. Barry, A. Jahangir, C. Finn, B. M. Buckley, and A. El-Gammal, "Comparison of arterial and venous blood gases and the effects of analysis delay and air contamination on arterial samples in patients with chronic obstructive pulmonary disease and healthy controls," *Respiration*, Vol. 81, no. 1, pp. 18–25, 2010.

95. Zonios, G., and A. Dimou, "Modeling diffuse reflectance from homogeneous semi-infinite turbid media for biological tissue applications: a Monte Carlo study," *Biomedical Optics Express*, Vol. 2, no. 12, p. 3284, 2011.

96. Zonios, G., I. Bassukas, and A. Dimou, "Comparative evaluation of two simple diffuse reflectance models for biological tissue applications," *Applied Optics*, Vol. 47, no. 27, pp. 4965–4973, 2008.

97. Zonios, G., and A. Dimou, "Simple two-layer reflectance model for biological tissue applications: Lower absorbing layer," *Applied Optics*, Vol. 49, no. 27, pp. 5026–5031, 2010.

98. Zonios, G., A. Dimou, I. Bassukas, D. Galaris, A. Tsolakidis, and E. Kaxiras, "Melanin absorption spectroscopy: new method for noninvasive skin investigation and melanoma detection," *Journal of Biomedical Optics*, Vol. 13, no. 1, 2008.

99. Marchesini, R., A. Bono, and M. Carrara, "In vivo characterization of melanin in melanocytic lesions: spectroscopic study on 1671 pigmented skin lesions," *Journal of Biomedical Optics*, Vol. 14, no. 1, 2009.

100. Zonios, G., A. Dimou, M. Carrara, and R. Marchesini, "In vivo optical properties of melanocytic skin lesions: Common nevi, dysplastic nevi and malignant melanoma," *Photochemistry and Photobiology*, Vol. 86, no. 1, pp. 236–240, 2010.

101. Sharma, V., J. W. He, S. Narvenkar, Y. B. Peng, and H. Liu, "Quantification of light reflectance spectroscopy and its application: Determination of hemodynamics on the rat spinal cord and brain induced by electrical stimulation," *NeuroImage*, Vol. 56, no. 3, pp. 1316–28, 2011.

102. Mantis, G., and G. Zonios, "Simple two-layer reflectance model for biological tissue applications," *Applied Optics*, Vol. 48, pp. 3490–3496, Jun. 2009.

103. Jacques, S. L., "Optical properties of biological tissues: A review," *Physics in Medicine and Biology*, Vol. 58, no. 11, pp. R37–61, 2013.

104. Mätzler, C., "Matlab Functions for Mie Scattering and Absorption," tech. rep., Universitas Bernensis, Institut für Angewandte Physik, https://omlc.org/spectra/hemoglobin/summary.html, 2002.

105. Hammer, M., D. Schweitzer, B. Michel, E. Thamm, and a. Kolb, "Single scattering by red blood cells," *Applied Optics*, 1998.

106. Hammer, M., A. N. Yaroslavsky, and D. Schweitzer, "A scattering phase function for blood with physiological haematocrit," *Physics in Medicine and Biology*, Vol. 46, no. 3, pp. N65–69, 2001.

107. Takatani, S., and M. D. Graham, "Theoretical analysis of diffuse reflectance from a two-layer tissue model," *IEEE Transactions on Biomedical Engineering*, Vol. BME-26, no. 12, pp. 656–664, 1979.

108. Schmitt, J. M., J. D. Meindl, and F. G. Mihm, "An integrated circuit-based optical sensor for in vivo measurement of blood oxygenation," *IEEE Transactions on Biomedical Engineering*, Vol. BME-33, no. 2, pp. 98–107, 1986.

109. Serebrennikova, Y. M., J. M. Smith, D. E. Huffman, G. F. Leparc, and L. H. García-Rubio, "Quantitative interpretations of Visible-NIR reflectance spectra of blood," *Optics Express*, Vol. 16, no. 22, p. 18215, 2008.

110. Steinke, J. M., and A. P. Shepherd, "Role of Light Scattering in Whole Blood Oximetry," *IEEE Transactions on Biomedical Engineering*, Vol. 33, no. 3, pp. 294–301, 1986.

111. Steinke, J. M., and A. P. Shepherd, "Diffusion model of the optical absorbance of whole blood," *Journal of the Optical Society of America A*, Vol. 5, no. 6, pp. 813–22, 1988.

112. Randeberg, L. L., *Diagnostic applications of diffuse reflectance spectroscopy*. PhD thesis, Norwegian University of Science and Technology, Trondheim, Norway, 2005.

113. Meinke, M., G. Müller, J. Helfmann, and M. Friebel, "Empirical model functions to calculate hematocrit-dependent optical properties of human blood," *Applied Optics*, Vol. 46, no. 10, pp. 1742–53, 2007.

114. Twersky, V., "Absorption and multiple scattering by biological suspensions," *Journal of the Optical Society of America*, Vol. 60, no. 8, pp. 1084–1093, 1970.

115. Hess, J. R., "Red cell storage," *Journal of Proteomics*, Vol. 73, no. 3, pp. 368–373, 2010.

116. Delobel, J., S. Barelli, G. Canellini, M. Prudent, N. Lion, and J.-D. Tissot, "Red blood cell microvesicles: a storage lesion or a possible salvage mechanism," *ISBT Science Series*, Vol. 11, no. S1, pp. 171–177, 2016.

117. Said, A. S., S. C. Rogers, and A. Doctor, "Physiologic impact of circulating RBC microparticles upon blood-vascular interactions," *Frontiers in Physiology*, Vol. 8, no. Jan., pp. 1–14, 2018.

118. Wang, L., and S. Jacques, "Monte Carlo Modeling of Light Ttransport in Multi-layered Tissues in Standard C," tech. rep., University of Texas, M. D. Anderson Cancer Center, https://omlc.org/classroom/ece532/class4/MCMan.pdf, 1992.

119. Meinke, M., I. Gersonde, M. Friebel, J. Helfmann, and G. Mu, "Chemometric determination of blood parameters using visible -near-infrared spectra," *Applied Spectroscopy*, Vol. 59, no. 6, pp. 826–835, 2005.

120. Zhang, S., G. Li, J. Wang, D. Wang, Y. Han, H. Cao, and L. Lin, "Nondestructive measurement of hemoglobin in blood bags based on multi-pathlength VIS-NIR Spectroscopy," *Scientific Reports*, Vol. 8, no. 1, pp. 1–9, 2018.

121. Steinke, J. M., and A. P. Shepherd, "Reflectance measurements of hematocrit and oxyhemoglobin saturation," *The American Journal of Physiology*, no. 1 Pt 2, pp. 147–153, 1987.

122. Can, O. M., Y. Ülgen, and H. Bilgen, "Monitoring Cole Parameters of Red Blood Cell Concentrates during Storage," in *International Workshop on Impedance Spectroscopy: Abstract Book*, (Chemnitz, Germany), p. 96, Chemnitz University of Technology, 24-27 Sept 2013.

123. Tuchin, V. V., *Handbook of Optical Biomedical Diagnostics*, Bellingham, Washingthon: SPIE Press, 2nd ed., 2002.

124. Cook, J. R., R. R. Bouchard, and S. Y. Emelianov, "Tissue-mimicking phantoms for photoacoustic and ultrasonic imaging," *Biomedical Optics Express*, Vol. 2, no. 11, pp. 3193–206, 2011.

125. Iizuka, M. N., M. D. Sherar, and I. A. Vitkin, "Optical phantom materials for near infrared laser photocoagulation studies," *Lasers in Surgery and Medicine*, Vol. 25, no. 2, pp. 159–169, 1999.

126. Royston, D. D., R. S. Poston, and S. A. Prahl, "Optical properties of scattering and absorbing materials used in the development of optical phantoms at 1064 nm," *Journal of Biomedical Optics*, Vol. 1, no. 1, pp. 110 – 116, 1996.

127. Svenmarker, P., C. T. Xu, S. Andersson-Engels, and J. Krohn, "Effects of probe geometry on transscleral diffuse optical spectroscopy," *Biomedical Optics Express*, Vol. 2, pp. 3058–3071, Nov 2011.

128. Pflaum, R. T., and A. I. Popov, "Inorganic salts in non-aqueous solvents. Absorption spectra of transition metal salts in dimethylformamide," *Analytica Chimica Acta*, Vol. 13, pp. 165–171, 1955.

129. Ninni, P. D., F. Martelli, and G. Zaccanti, "The use of india ink in tissue-simulating phantoms," *Optics Express*, Vol. 18, pp. 26854–26865, Dec. 2010.

130. Bashkatov, A. N., E. A. Genina, V. I. Kochubey, and et. al., "Optical properties of melanin in the skin and skin like phantoms," in *Controlling Tissue Optical Properties: Applications in Clinical Study* (Tuchin, V. V., ed.), Vol. 4162, pp. 219 – 226, International Society for Optics and Photonics, SPIE, 2000.

131. Sekar, S. K. V., A. Pacheco, P. Martella, H. Li, P. Lanka, A. Pifferi, and S. Andersson-Engels, "Solid phantom recipe for diffuse optics in biophotonics applications: a step towards anatomically correct 3D tissue phantoms," *Biomedical Optics Express*, Vol. 10, no. 4, pp. 2090–2100, 2019.

132. Pogue, B. W., and M. S. Patterson, "Review of tissue simulating phantoms for optical spectroscopy, imaging and dosimetry," *Journal of Biomedical Optics*, Vol. 11, no. 4, 2006.

133. Flock, S. T., S. L. Jacques, B. C. Wilson, W. M. Star, and M. J. C. Van Gemert, "Optical properties of intralipid: A phantom medium for light propagation studies," *Lasers in Surgery and Medicine*, Vol. 12, no. 5, pp. 510–519, 1992.

134. Spinelli, L., M. Botwicz, N. Zolek, and et. al., "Determination of reference values for optical properties of liquid phantoms based on Intralipid and India ink," *Biomedical Optics Express*, Vol. 5, no. 7, pp. 2037–2053, 2014.

135. Cugmas, B., P. Naglic, S. Menachery, F. Pernuš, and B. Likar, "Poor optical stability of molecular dyes when used as absorbers in water-based tissue-simulating phantoms," *Design and Quality for Biomedical Technologies XII*, no. Feb., 2019.

136. Landsman, M. L., G. Kwant, G. A. Mook, and W. G. Zijlstra, "Light absorbing properties, stability, and spectral stabilization of indocyanine green," *Journal of Applied Physiology*, Vol. 40, no. 4, pp. 575–583, 1976.

137. Akarçay, H. G., S. Preisser, M. Frenz, and J. Rička, "Determining the optical properties of a gelatin TiO_2 phantom at 780 nm," *Biomedical Optics Express*, Vol. 3, no. 3, pp. 418–434, 2012.

138. Jones, C. J. M., and P. R. T. Munro, "Stability of gel wax based optical scattering phantoms," *Biomedical Optics Express*, Vol. 9, no. 8, pp. 3495–3502, 2018.

139. Krauter, P., S. Nothelfer, N. Bodenschatz, E. Simon, F. Foschum, and A. Kienle, "Adjusting subdiffusive parameters in optical phantoms," in *Diffuse Optical Imaging V* (Dehghani, H., and P. Taroni, eds.), Vol. 9538, (Munich, Germany), pp. 74–78, SPIE-OSA, 2015.

140. Saager, R. B., A. Quach, R. A. Rowland, M. L. Baldado, and A. J. Durkin, "Low-cost tissue simulating phantoms with adjustable wavelength-dependent scattering properties in the visible and infrared ranges," *Journal of Biomedical Optics*, Vol. 21, no. 6, 2016.

141. Qin, J., and R. Lu, "Hyperspectral diffuse reflectance imaging for rapid, noncontact measurement of the optical properties of turbid materials," *Applied Optics*, Vol. 45, pp. 8366–8373, Nov. 2006.

142. Bevilacqua, F., P. Marquet, O. Coquoz, and C. Depeursinge, "Role of tissue structure in photon migration through breast tissues," *Applied Optics*, Vol. 36, no. 1, pp. 44–51, 1997.

143. Li, C., and H. Jiang, "Measurement of particle-size distribution and concentration in heterogeneous turbid media with multispectral diffuse optical tomography," *Applied Optics*, Vol. 44, pp. 1838–1844, Apr. 2005.

144. Nivetha, K. B., and N. Sujatha, "Development of thin skin mimicking bilayer solid tissue phantoms for optical spectroscopic studies," *Biomedical Optics Express*, Vol. 8, no. 7, pp. 3198–3212, 2017.

145. Di Ninni, P., Y. Bérubé-Lauzière, L. Mercatelli, E. Sani, and F. Martelli, "Fat emulsions as diffusive reference standards for tissue simulating phantoms?," *Applied Optics*, Vol. 51, no. 30, pp. 7176–7182, 2012.

146. van Staveren, H. J., C. J. M. Moes, J. van Marie, S. A. Prahl, and M. J. C. van Gemert, "Light scattering in lntralipid-10% in the wavelength range of 400-1000 nm," *Applied Optics*, Vol. 30, no. 31, pp. 4507–4514, 1991.

147. Aernouts, B., R. V. Beers, R. Watté, J. Lammertyn, and W. Saeys, "Dependent scattering in intralipid® phantoms in the 600-1850 nm range," *Optics Express*, Vol. 22, pp. 6086–6098, Mar. 2014.

148. Ninni, P. D., F. Martelli, and G. Zaccanti, "Effect of dependent scattering on the optical properties of intralipid tissue phantoms," *Biomedical Optics Express*, Vol. 2, pp. 2265–2278, Aug. 2011.

149. Franceschini, M. A., S. Fantini, A. Cerussi, B. Barbieri, B. Chance, and E. Gratton, "The effect of water in the quantitation of hemoglobin concentration in a tissue-like phantom by near-infrared spectroscopy," in *Biomedical Optical Spectroscopy and Diagnostics*, no. AP16, Optical Society of America, 1996.

150. Heine, M., F. Foschum, and A. Kienle, "Determination of the optical properties of anisotropic turbid media using an integrating sphere," in *Clinical and Biomedical Spectroscopy*, no. 7368-1U, (Munich, Germany), SPIE, OSA, 2009.

151. Michels, R., F. Foschum, and A. Kienle, "Optical properties of fat emulsions," *Optics Express*, Vol. 16, no. 8, pp. 5907–25, 2008.

152. Aernouts, B., E. Zamora-Rojas, R. Van Beers, R. Watté, L. Wang, M. Tsuta, J. Lammertyn, and W. Saeys, "Supercontinuum laser based optical characterization of Intralipid® phantoms in the 500-2250 nm range," *Optics Express*, Vol. 21, no. 26, pp. 32450–32467, 2013.

153. Raju, M., and S. N. Unni, "Concentration-dependent correlated scattering properties of Intralipid 20% dilutions," *Applied Optics*, Vol. 56, no. 4, pp. 1157–1166, 2017.

154. Zaccanti, G., S. Del Bianco, and F. Martelli, "Measurements of optical properties of high-density media," *Applied Optics*, Vol. 42, no. 19, pp. 4023–4030, 2003.

155. Mourant, J. R., T. Fuselier, J. Boyer, T. M. Johnson, and I. J. Bigio, "Predictions and measurements of scattering and absorption over broad wavelength ranges in tissue phantoms," *Applied Optics*, Vol. 36, no. 4, pp. 949–57, 1997.

156. Moes, C. J. M., M. J. C. van Gemert, W. M. Star, J. P. A. Marijnissen, and S. A. Prahl, "Measurements and calculations of the energy fluence rate in a scattering and absorbing phantom at 633 nm," *Applied Optics*, Vol. 28, no. 12, pp. 2292–6, 1989.

157. Dam, J. S., C. B. Pedersen, T. Dalgaard, P. E. Fabricius, P. Aruna, and S. Andersson-Engels, "Fiber-optic probe for noninvasive real-time determination of tissue optical properties at multiple wavelengths," *Applied Optics*, Vol. 40, pp. 1155–1164, Mar. 2001.

158. Shrivastava, A., and V. Gupta, "Methods for the determination of limit of detection and limit of quantitation of the analytical methods," *Chronicles of Young Scientists*, Vol. 2, no. 1, pp. 21–5, 2011.